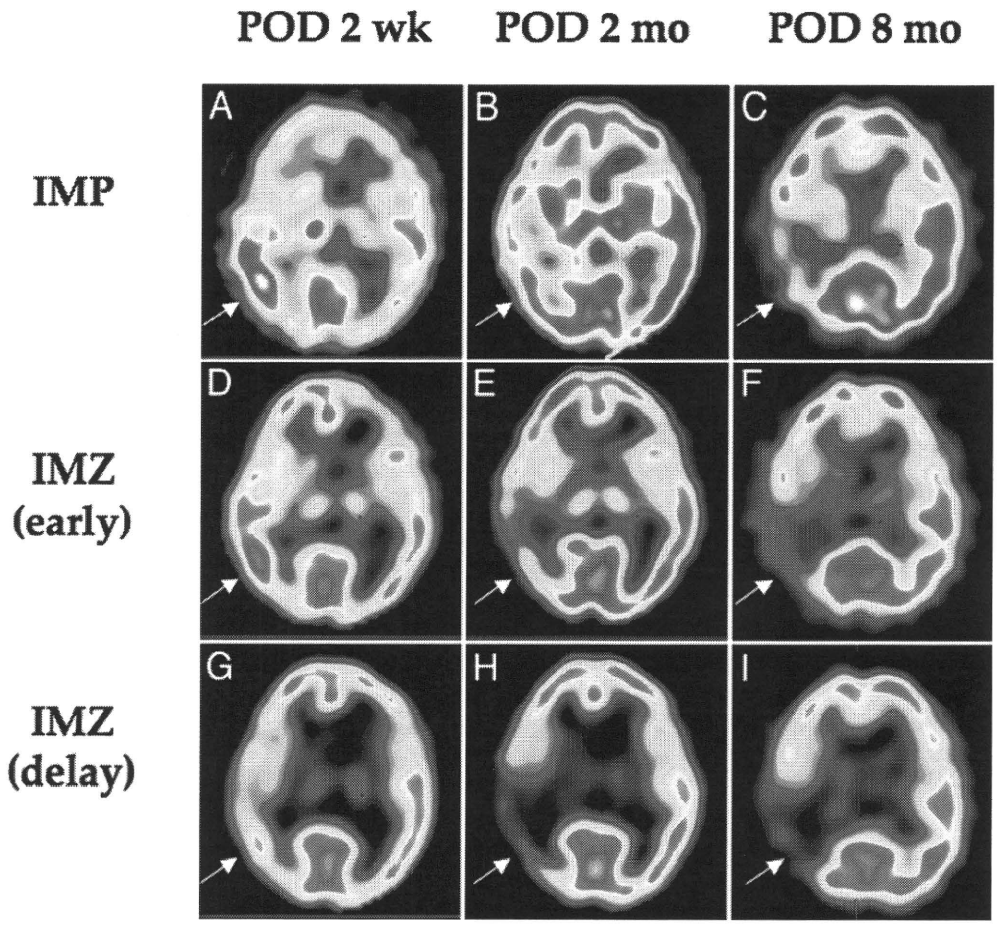

Fig. 2. Chronological changes in ^{123}I-IMP and early and delayed ^{123}I-IMZ SPECT images. Iodine-123–labeled iodoamphetamine **(A–C)** and early ^{123}I-IMZ **(D–F)** images similarly showing a transient increase in the subacute stage (POD 2 weeks [POD 2 wk; **A and D**]), followed by progressive decrease in the early and late chronic stages (POD 2 months [POD 2 mo; **B and E**] and 8 months [POD 8 mo; **C and F**]) of uptake in the affected regions. Delayed images of ^{123}I-IMZ **(G–I)** demonstrating delayed decrease of binding of the affected regions between subacute **(G)** and early chronic **(H)** stages, which levels off in the late chronic stage **(I)**. *Arrows* indicate the affected region in the temporal lobe.

affected cortex on PODs 1 and 7 in this case, as reported in global ischemia,[11] disappeared thereafter, despite ongoing neuronal loss during the subacute stage. In animal models, modest signal intensity changes on diffusion weighted imaging precede delayed neuronal necrosis after transient ischemia.[15] In the present case, however, the rate of decrease of the affected/unaffected ratio, as seen on the delayed ^{123}I-IMZ images, remained constant until POD 55 before and after the first postoperative ^{123}I-IMZ image, if the affected/unaffected ratio before surgery in

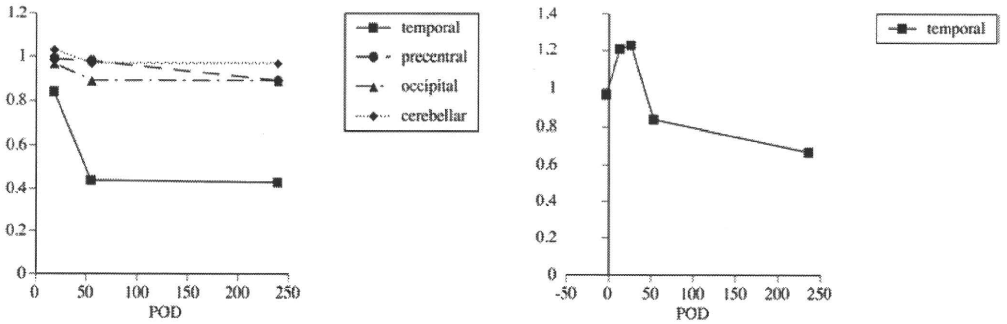

Fig. 3. Line graphs depicting chronological changes of the affected/unaffected count ratio and corresponding regions of interest on delayed ^{123}I-IMZ ***(left)*** and ^{123}I-IMP ***(right)*** SPECT images. The count ratio of the affected/unaffected corresponding regions of interest of ^{123}I-IMZ in the different areas (temporal, precentral, occipital, and cerebellar regions) are plotted against PODs. The affected/unaffected ratio of ^{123}I-IMP was plotted only for the affected temporal region.

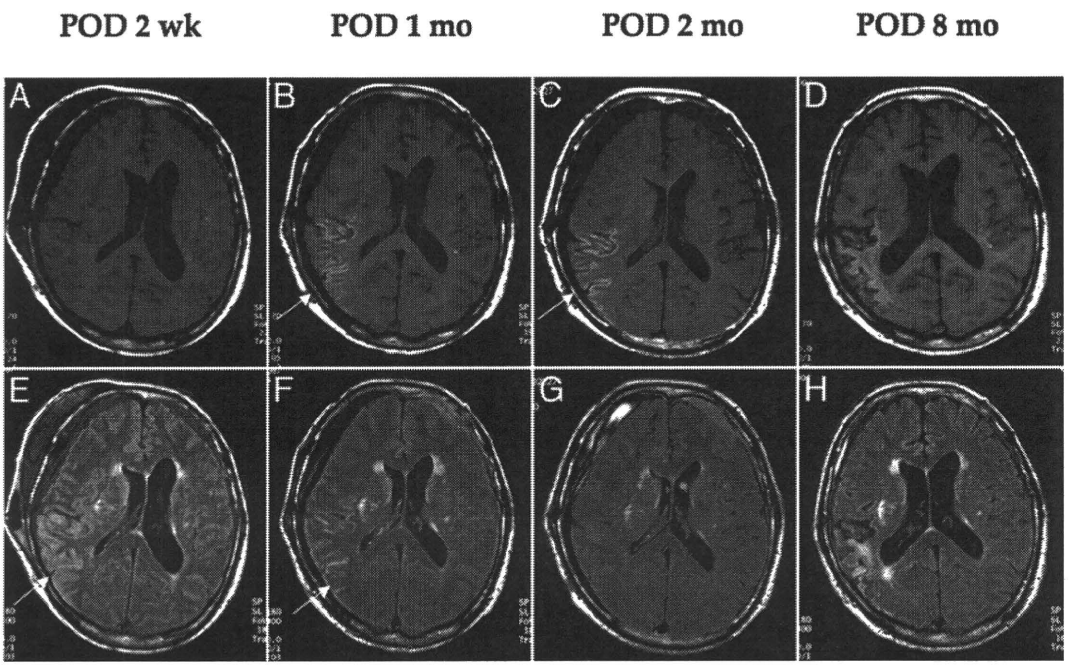

Fig. 4. Chronological changes demonstrated on follow-up MR images. Sagittal T1-weighted images **(A–D)** showing emerging cortical hyperintensity of the affected cortex between 2 weeks after surgery (POD 2 wk; **A**) and 1 month after surgery (POD 1 mo; **B**); the hyperintensity becomes more prominent at 2 months (POD 2 mo; **C**). Cortical laminar necrosis indicates atrophic change in the late chronic stage **(D)**. **E–H:** On FLAIR images, cortical hyperintensity gradually decreases from 2 weeks after surgery (POS 2 wk; **E**) to 1 month after surgery (POD 1 mo; **F**) postoperatively and almost disappears by 2 months (POD 2 mo; **G**). In the late chronic stage, cortical atrophy with secondary degeneration of the underlying subcortical white matter is noted **(H)**.

the affected cortex was assumed to be 1.0, as in the other areas on the first postoperative ^{123}I-IMZ image. These findings suggest that neuronal loss may not be of delayed onset, but rather slowly progressive after surgery, and diffusion weighted and ^{123}I-IMZ imaging may differ in predicting the probability of slowly progressive neuronal death in cortical laminar necrosis, depending on the interval from the moderate ischemic insult. Iodine-123–labeled IMZ SPECT is useful for examining the dynamic process of slowly progressive neuronal loss, especially in the subacute phase after moderate ischemia. Precise understanding of temporal profiles of neuronal death underlying emerging cortical laminar necrosis should require further accumulation of evidence using ^{123}I-IMZ SPECT.

Previous studies discussed the time permitted for temporary occlusion of the parent artery for aneurysm surgery, especially for an MCA bifurcation aneurysm.[8,12,14] In radial artery/ECA-MCA bypass grafting, however, the time permitted for temporary occlusion of the M_2 segment remains unclear, although the anastomotic time has been recommended to be less than 45 minutes.[12] Obviously, the time threshold for temporary occlusion may depend on multiple factors, such as the use of various neuroprotective agents,[8,14] brain temperature,[21] and extent of collateral flow and cerebrovascular reserve. During the previous 6 years, neither isolated cortical laminar necrosis nor frank infarction due to temporary occlusion had been documented in the other 21 cases treated by high-flow bypass, including 10 patients in whom temporary occlusion lasted more than 45 minutes. In the present case, extremely slow backflow from the distal side of the clamped artery was a key intraoperative finding, underlying the development of slowly progressive neuronal death. Although previous studies have reported possible preventative measures of ischemic complications related to temporary occlusion, such as excimer laser–assisted nonocclusive anastomosis,[18] the development of small intravascular shunts,[12] and double insurance bypass,[5] there are no widely accepted methods for this purpose.

Conclusions

We have discussed a rare case of slowly progressive neuronal death during postischemic hyperperfusion in cortical laminar necrosis associated with radial artery/ECA-MCA bypass grafting for intracavernous CA aneurysms. We have illustrated the diagnostic importance using of ^{123}I-IMZ SPECT in the subacute phase before emerging characteristic MR imaging findings. Moderate ischemia during temporary occlusion due to poor collateral flow may cause this rare ischemic complication.

Disclaimer

The authors report no conflict of interest concerning the materials or methods used in this study or the findings specified in this paper.

Acknowledgments

The authors thank Drs. Hiroshi Moriwaki, Kazuyuki Nagatsuka, and Kazunori Toyoda (Cerebrovascular Division, Department of Internal Medicine, National Cardiovascular Center); Masaki

Komiyama (Department of Neurosurgery, Osaka City General Hospital); and Shobu Namura (Department of Anatomy and Neurobiology, Morehouse School of Medicine) for helpful discussion, as well as Masaji Fukumoto (National Cardiovascular Center) for analyzing the data of ^{123}I-IMZ and ^{123}I-IMP SPECT.

References

1. Garcia JH, Liu KF, Ye ZR, Gutierrez JA: Incomplete infarct and delayed neuronal death after transient middle cerebral artery occlusion in rats. **Stroke 28:**2303–2310, 1997
2. Hantraye P, Kaijima M, Prenant C, Guibert B, Sastre J, Crouzel M, et al: Central type benzodiazepine binding sites: a positron emission tomography study in the baboon's brain. **Neurosci Lett 48:**115–120, 1984
3. Heiss WD, Grond M, Thiel A, Ghaemi M, Sobesky J, Rudolf J, et al: Permanent cortical damage detected by flumazenil positron emission tomography in acute stroke. **Stroke 29:**454–461, 1998
4. Heiss WD, Sobesky J, Smekal U, Kracht LW, Lehnhardt FG, Thiel A, et al: Probability of cortical infarction predicted by flumazenil binding and diffusion-weighted imaging signal intensity: a comparative positron emission tomography/magnetic resonance imaging study in early ischemic stroke. **Stroke 35:**1892–1898, 2004
5. Hongo K, Horiuchi T, Nitta J, Tanaka Y, Tada T, Kobayashi S: Double-insurance bypass for internal carotid artery aneurysm surgery. **Neurosurgery 52:**597–602, 2003
6. Jafar JJ, Russell SM, Woo HH: Treatment of giant intracranial aneurysms with saphenous vein extracranial-to-intracranial bypass grafting: indications, operative technique, and results in 29 patients. **Neurosurgery 51:**138–146, 2002
7. Komiyama M, Nakajima H, Nishikawa M, Yasui T: Serial MR observation of cortical laminar necrosis caused by brain infarction. **Neuroradiology 40:**771–777, 1998
8. Lavine SD, Masri LS, Levy ML, Giannotta SL: Temporary occlusion of the middle cerebral artery in intracranial aneurysm surgery: time limitation and advantage of brain protection. **J Neurosurg 87:**817–824, 1997
9. Lawton MT, Hamilton MG, Morcos JJ, Spetzler RF: Revascularization and aneurysm surgery: current techniques, indications, and outcome. **Neurosurgery 38:**83–84, 1996
10. Marchal G, Young AR, Baron JC: Early postischemic hyperperfusion: pathophysiologic insights from positron emission tomography. **J Cereb Blood Flow Metab 19:**467–482, 1999
11. McKinney AM, Teksam M, Felice R, Casey SO, Cranford R, Truwit CL, et al: Diffusion-weighted imaging in the setting of diffuse cortical laminar necrosis and hypoxic-ischemic encephalopathy. **AJNR Am J Neuroradiol 25:**1659–1665, 2004
12. Mohit AA, Sekhar LN, Natarajan SK, Britz GW, Ghodke B: High-flow bypass grafts in the management of complex intracranial aneurysms. **Neurosurgery 60 (2 Suppl 1):**ONS105–ONS123, 2007
13. Nakagawara J, Sperling B, Lassen NA: Incomplete brain infarction of reperfused cortex may be quantitated with iomazenil. **Stroke 28:**124–132, 1997
14. Ogilvy CS, Carter BS, Kaplan S, Rich C, Crowell RM: Temporary vessel occlusion for aneurysm surgery: risk factors for stroke in patients protected by induced hypothermia and hypertension and intravenous mannitol administration. **J Neurosurg 84:**785–791, 1996
15. Rojas S, Martin A, Justicia C, Falcon C, Bargallo N, Chamorro A, et al: Modest MRI signal intensity changes precede delayed cortical necrosis after transient focal ischemia in the rat. **Stroke 37:**1525–1532, 2006
16. Sette G, Baron JC, Young AR, Miyazawa H, Tillet I, Barre L, et al: In vivo mapping of brain benzodiazepine receptor changes by positron emission tomography after focal ischemia in the anesthetized baboon. **Stroke 24:**2046–2048, 1993
17. Siskas N, Lefkopoulos A, Ioannidis I, Charitandi A, Dimitriadis AS: Cortical laminar necrosis in brain infarcts: serial MRI. **Neuroradiology 45:**283–288, 2003
18. Streefkerk HJ, Bremmer JP, Tulleken CA: The ELANA technique: high flow revascularization of the brain. **Acta Neurochir Suppl 94:**143–148, 2005
19. Takahashi S, Higano S, Ishii K, Matsumoto K, Sakamoto K, Iwasaki Y, et al: Hypoxic brain damage: cortical laminar necrosis and delayed changes in white matter at sequential MR imaging. **Radiology 189:**449–456, 1993
20. Weiller C, Willmes K, Reiche W, Thron A, Isensee C, Buell U, et al: The case of aphasia or neglect after striatocapsular infarction. **Brain 116:**1509–1525, 1993
21. Westermaier T, Zausinger S, Baethmann A, Steiger HJ, Schmid-Elsaesser R: No additional neuroprotection provided by barbiturate-induced burst suppression under mild hypothermic conditions in rats subjected to reversible focal ischemia. **J Neurosurg 93:**835–844, 2000
22. Yamauchi H, Kudoh T, Kishibe Y, Iwasaki J, Kagawa S: Selective neuronal damage and borderzone infarction in carotid artery occlusive disease: a 11C-flumazenil PET study. **J Nucl Med 46:**1973–1979, 2005

Manuscript submitted March 2, 2009.
Accepted September 28, 2009.
Please include this information when citing this paper: published online October 30, 2009; DOI: 10.3171/2009.9.JNS09345.
Address correspondence to: Koji Iihara, M.D., Ph.D., Department of Neurosurgery, National Cardiovascular Center, 5-7-1 Fujishirodai, Suita, Osaka 565-8565, Japan. email: kiihara@hsp.ncvc.go.jp.

Journal of Cerebral Blood Flow & Metabolism (2010) 30, 663–673

www.jcbfm.com

Measurement of density and affinity for dopamine D_2 receptors by a single positron emission tomography scan with multiple injections of [^{11}C]raclopride

Yoko Ikoma[1,2], Hiroshi Watabe[1], Takuya Hayashi[1], Yoshinori Miyake[1], Noboru Teramoto[1], Kotaro Minato[2] and Hidehiro Iida[1]

[1]*Department of Investigative Radiology, National Cardiovascular Center Research Institute, Osaka, Japan;* [2]*Biomedical Imaging and Informatics, Graduate School of Information Science, Nara Institute of Science and Technology, Nara, Japan*

Positron emission tomography (PET) with [^{11}C]raclopride has been used to investigate the density (B_{max}) and affinity (K_d) of dopamine D_2 receptors related to several neurological and psychiatric disorders. However, in assessing the B_{max} and K_d, multiple PET scans are necessary under variable specific activities of administered [^{11}C]raclopride, resulting in a long study period and unexpected physiological variations. In this paper, we have developed a method of multiple-injection graphical analysis (MI-GA) that provides the B_{max} and K_d values from a single PET scan with three sequential injections of [^{11}C]raclopride, and we validated the proposed method by performing numerous simulations and PET studies on monkeys. In the simulations, the three-injection protocol was designed according to prior knowledge of the receptor kinetics, and the errors of B_{max} and K_d estimated by MI-GA were analyzed. Simulations showed that our method could support the calculation of B_{max} and K_d, despite a slight overestimation compared with the true magnitudes. In monkey studies, we could calculate the B_{max} and K_d of diseased or normal striatum in a 150 mins scan with the three-injection protocol of [^{11}C]raclopride. Estimated B_{max} and K_d values of D_2 receptors in normal or partially dopamine-depleted striatum were comparable to the previously reported values.

Journal of Cerebral Blood Flow & Metabolism (2010) **30,** 663–673; doi:10.1038/jcbfm.2009.239; published online 11 November 2009

Keywords: [^{11}C]raclopride; dopamine D_2 receptors; graphical analysis; multiple injections; positron emission tomography

Introduction

Positron emission tomography (PET) with [^{11}C]raclopride has been widely used to investigate the availability of striatal dopamine D_2 receptors *in vivo* (Farde *et al*, 1985; Köhler *et al*, 1985; Hall *et al*, 1988). A number of postmortem studies have shown that the abundance of dopamine D_2 receptor is elevated in striatum samples from untreated patients with Parkinson's disease (Guttman and Seeman, 1985; Seeman *et al*, 1987) and in schizophrenic patients who had never taken antipsychotics (Cross *et al*, 1981; Joyce *et al*, 1988). The PET measurements have made it possible to quantify *in vivo* the density and apparent affinity of receptors by systematically varying the specific activity (or mass) of an administered radioligand (see for example, Farde *et al*, 1986). A study of Parkinson's disease by Rinne *et al* (1995) with *in vivo* PET showed increased density and unchanged affinity of dopamine D_2 receptors in the putamen in comparison with healthy controls. In corresponding studies of schizophrenia, early findings with [^{11}C]*N*-methylspiperone indicated elevated D_2 binding, which was not replicated in some subsequent studies with [^{11}C]raclopride (Wong *et al*, 1986; Farde *et al*, 1987, 1990). Dysfunction of dopamine receptors has also been suggested in other neurodegenerative or psychiatric diseases (e.g., multiple-system atrophy, progressive supranuclear palsy, and attention-deficit hyperactivity disorders); however, there have been only a few studies that

Correspondence: Dr H Watabe, Department of Investigative Radiology, National Cardiovascular Center Research Institute, 5-7-1, Fujishirodai, Suita, Osaka 565-8565, Japan.
E-mail: watabe@ri.ncvc.go.jp
Received 11 September 2009; revised 13 October 2009; accepted 19 October 2009; published online 11 November 2009

examined receptor function directly related to density and affinity. This might be due to the inherent difficulty in measuring absolute receptor abundance based on PET recordings.

In PET scans, to determine the density and affinity of receptors directly as parameters of kinetic model, it is necessary to apply a compartmental analysis based on a two-tissue compartment five-parameter model including density of receptors B_{max} (pmol/mL), bimolecular association rate constant k_{on} (mL/pmol/min), and unimolecular dissociation rate constant k_{off} (min^{-1}) (Farde *et al*, 1989). However, since data from a single PET scan are not enough to determine the B_{max} and k_{on} individually, multiple PET scans should be taken with different molar amounts of injected ligand. In addition, model parameters are estimated by a nonlinear least squares fitting with the metabolite-corrected plasma input function, so the solutions are often unstable and sensitive to statistical noise, and invasive arterial sampling is required to use this method.

Farde *et al* (1986, 1989) determined the value of B_{max} and apparent affinity K_d ($=k_{off}/k_{on}$) by a graphical analysis using a time-activity curve (TAC) of the specifically bound target region and a reference region where specific bindings are negligible. In this method, the ratio of specific bound and free ligand concentrations at the equilibrium state are plotted versus the concentration of specific bound ligand, and B_{max} and K_d are estimated from the slope and intercept of the regression line. Other groups also used the value of distribution volume ratio − 1 estimated from the graphical analysis of Logan *et al* (1996), instead of the ratios of specific bound and free concentration, to obtain stable values of the *y*-axis quantity (Logan *et al*, 1997; Doudet and Holden, 2003; Doudet *et al*, 2003). These methods are practical, because they do not require arterial blood sampling, and their respective estimation processes are easy to carry out. However, to estimate the regression line of a graphical plot, multiple PET scans (at least two or three) are required under variable molar amounts of administered ligand, so scans have been performed on separate days. Even in quantitative PET scans, the separate day protocol may suffer from interday or intraday variations in physiologic conditions, such as cerebral blood pressure, flow, and receptor bindings, which may affect the accuracy of the estimates.

We developed a method, called the multiple-injection simplified reference tissue model (MI-SRTM), to measure the change in binding potential ($BP_{ND}=k_3/k_4$ (Mintun *et al*, 1984)) of dopamine D_2 receptors from a single session of PET scanning with multiple injections of [^{11}C]raclopride (Watabe *et al*, 2006; Ikoma *et al*, 2009), and we showed that this method could detect the change in BP_{ND} because of an increase in mass of administered [^{11}C]raclopride in a short scanning period, which is a prerequisite for measuring the saturation binding parameters as steady state. In this study, we extend our earlier report for estimating B_{max} and K_d from a single session of PET scanning with triple injections of [^{11}C]raclopride using MI-SRTM and the graphical analysis, and we validated the proposed method by performing numerous simulations and studies on monkeys using PET and [^{11}C]raclopride.

Materials and methods

Theory

Graphical Analysis with a Reference Region for Estimation of Density and Affinity: Graphical analysis based on the Scatchard plot (Scatchard, 1949) has been used to estimate the values of B_{max} and K_d from as series of PET recordings with various molar amounts of administered ligand (Farde *et al*, 1986). In brief, the ratios (B/F) of specific bound ligand concentration (B [pmol/mL]) and free ligand concentration (F [pmol/mL]) at equilibrium are plotted versus B. In this plot, the slope and *x*-intercept represent $-1/K_d$ and B_{max}, respectively. In general, for graphical analysis without arterial blood sampling, the total radioligand concentration in the reference region (C_r [Bq/mL]), where specific bindings are negligible, is used as an estimate of the free radioligand concentration in the target region (C_f [Bq/mL]), that is $C_f^{ref}=C_r$, and the specific binding radioligand concentration in the target region (C_b [Bq/mL]) is defined as radioactivity in the target region (C_t [Bq/mL]) reduced with C_r, that is $C_b^{ref}=C_t-C_r$ (Figure 1). The radioactivity concentrations of C_f^{ref} and C_b^{ref}, at the point in time when dC_b^{ref}/dt is 0 (T_{eq}), are divided by a specific activity of the administered ligand, and used as F and B at the transient equilibrium in the graphical analysis

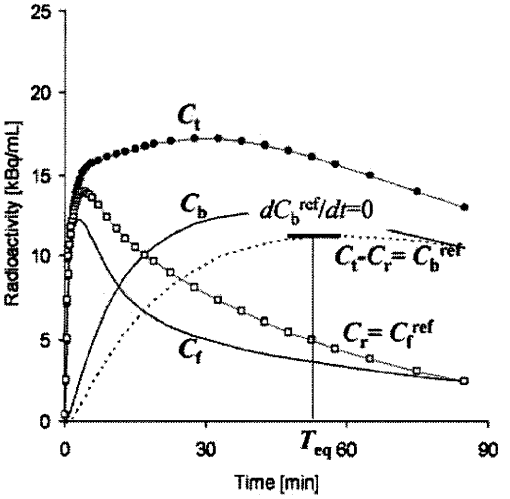

Figure 1 An example of simulated TACs for the striatum (C_t), free (C_f), and specific bound (C_b) concentrations in the striatum, the cerebellum used as a reference region (C_r) and bound concentration in the striatum estimated using a reference region ($C_b^{ref}=C_t-C_r$) with $K_1=0.033$, $K_1/k_2=0.59$, $k_{on}=0.0033$, $B_{max}=25.7$, $k_4=0.034$ for the striatum, and $K_1=0.034$, $K_1/k_2=0.36$, $k_3=0.022$, $k_4=0.034$ for the cerebellum. The time point of $dC_b^{ref}/dt=0$ (T_{eq}) is considered the transient equilibrium, and bound concentration at the equilibrium (B^{ref}) is obtained from the radioactivity concentration of C_b^{ref} at T_{eq}.

(Farde *et al*, 1989). In our study, we use the nomenclature B^{ref} and F^{ref} to represent the concentrations otherwise known as B and F. The value of the y axis, B^{ref}/F^{ref}, is sometimes replaced by the binding potential estimated by the graphical analysis of Logan *et al* (1996) or some other method (Logan *et al*, 1997; Doudet and Holden, 2003; Doudet *et al*, 2003).

Multiple-Injection Simplified Reference Tissue Model for Estimation of Binding Potential: A simplified reference tissue model (SRTM) can provide three parameters (R_1, k_2, BP_{ND}) without invasive arterial blood sampling by using a TAC of the reference region (Lammertsma and Hume, 1996). The MI-SRTM extended this SRTM for sequential multiple injections in a single session of PET scanning by taking into account the residual radioactivity in the target tissue at the time of each injection. As such, the magnitude of BP_{ND} for the ith injection is described in the following terms (Ikoma *et al*, 2009):

$$C_{ti}(t) = R_{1i}C_{ri}(t) + \left(k_{2i} - \frac{R_{1i}k_{2i}}{1+\mathrm{BP_{NDi}}}\right)e^{-\frac{k_{2i}}{1+\mathrm{BP_{NDi}}}t} \otimes C_{ri}(t) + (C_{ti}(0) - R_{1i}C_{ri}(0))e^{-\frac{k_{2i}}{1+\mathrm{BP_{NDi}}}t} \quad (1)$$

where C_{ti} and C_{ri} are the radioactivity concentrations in the target and reference region, respectively, and t is the time from the start of the ith injection.

Multiple-Injection Graphical Analysis for Estimation of Density and Affinity: The conventional graphical analysis was applied to the B_{max} and K_d estimations with the multiple-injection approach. In this multiple-injection graphical analysis (MI-GA), the BP_{ND} calculated for each injection using MI-SRTM was plotted as a function of the concentration of specific bound raclopride at the transient equilibrium (B^{ref} [pmol/mL]) within the scan duration for each injection, and B_{max} and K_d were estimated from the regression line.

In this study for [^{11}C]raclopride, the TAC of the cerebellum was used as the reference TAC. Each parameter in the MI-SRTM was estimated by nonlinear least squares fitting with iteration of the Gauss–Newton algorithm. It should be noted that the transient equilibrium condition is required for each injection in the MI-GA.

Simulation Analysis

Simulations were performed to determine the range of administered mass of three injections and to evaluate feasibility of the MI-GA to estimate the B_{max} and K_d.

Effect of Injected Mass on BP_{ND} Estimates: To investigate the effect of the administered molar amount of [^{11}C]raclopride on BP_{ND} estimates and to determine the molar amount of three injections for monkey studies, a relationship between BP_{ND} and B^{ref} was obtained by a computer simulation. Noiseless TACs of the striatum and cerebellum were generated with a measured plasma TAC and assumed parameter values derived from measurements taken from the monkey studies. The TAC of the cerebellum was simulated with a conventional two-tissue compartment four-parameter model with assumed parameter values obtained earlier in our monkey studies: $K_1 = 0.034$ (mL/mL/min) $K_1/k_2 = 0.36$, $k_3 = 0.022$ (min^{-1}), $k_4 = 0.034$ (min^{-1}). Meanwhile, the TAC of the striatum was simulated with a two-tissue compartment five-parameter model expressed as Equation (2) by solving these differential equations with the numerical analysis of fourth-order Runge–Kutta method with assumed parameter values $K_1 = 0.033$ (mL/mL/min), $K_1/k_2 = 0.59$, $k_{on} = 0.0033$ (mL/pmol/min), $B_{max} = 25.7$ (pmol/mL), $k_4 = 0.026$ (min^{-1}), and SA = 37 (GBq/μmol):

$$\begin{aligned} \frac{dC_f}{dt} &= K_1 C_p(t) - \left(k_2 + k_3'(t)\right)C_f(t) + k_4 C_b(t) \\ \frac{dC_b}{dt} &= k_3'(t)C_f(t) - k_4 C_b(t) \\ k_3'(t) &= k_{on}\left(B_{max} - \frac{C_b(t)}{SA}\right) \end{aligned} \quad (2)$$

where C_f and C_b are the concentrations of radioactivity for free and specifically bound [^{11}C]raclopride in tissue, respectively; and SA is the specific activity of administered [^{11}C]raclopride.

As reference, the relationships between B^{ref} and BP_{ND} or B^{ref}/F^{ref} were investigated in the case of a single injection of [^{11}C]raclopride by varying injected mass. TACs of the striatum and cerebellum for the single injection with a 50 mins scan were generated using the measured plasma TAC of a single injection in which the input plasma TAC was amplified, such that the corresponding mass increased from 1 to 500 nmol per injection. In each simulated TAC, BP_{ND} values were estimated by the SRTM, and then, B^{ref}/F^{ref} and B^{ref} were calculated by the transient equilibrium with the cerebellum TAC.

Next, TACs of the striatum and cerebellum for three injections at 50 mins intervals were generated using the plasma TAC of three sequential injections in which the input plasma TAC was amplified so that the mass of the first and second injections would be 1.5 and 10 nmol/kg, and the mass of the third injection would be 1.5 to 150 nmol/kg. In each simulated TAC, BP_{ND} values were estimated by the MI-SRTM, and B^{ref}/F^{ref} and B^{ref} for the third injection was calculated by the transient equilibrium with the cerebellum TAC. The relationships between B^{ref} and BP_{ND} or B^{ref}/F^{ref} for the third injection were investigated, and compared with that for the single injection.

Estimation of B_{max} and K_d Values by the Multiple-Injection Graphical Analysis: The reliability of B_{max} and K_d estimates by the graphical analysis was investigated for the proposed sequential multiple-injection approach (single PET scan) and compared with that for the conventional nonsequential approach (three PET scans on different days, such that no residual mass remained). Noiseless TACs of the striatum and cerebellum were simulated using assumed parameters of the two-tissue compartment model mentioned above and the plasma input function for three injections in which the magnitude of each 'virtual' input function was adjusted so that the injection mass would be 1.5, 10, or 30 nmol/kg determined from the simulation study mentioned above, with 50 mins intervals as reported

by Ikoma *et al* (2009). In the striatum TACs, B_{max} values were varied from 10 to 50 pmol/mL at 5 pmol/mL intervals with other parameters fixed (K_d = 7.9 pmol/mL), or K_d was varied from 3 to 15 at 2 pmol/mL intervals by changing k_{on} with other parameters fixed (B_{max} = 25.7 pmol/mL). For each TAC, B_{max} and K_d were estimated by the MI-GA from three points obtained by MI-SRTM for the single PET scan approach and they were estimated by the graphical analysis from three points obtained by the conventional SRTM for the three PET scan approach. Then, estimates were compared with the true values. In the single PET scan approach, B_{max} and K_d were also estimated without reference TAC by the MI-GA from three points of BP_{ND} and B obtained by the two-tissue compartment four-parameter model with the plasma input function shown in the Appendix.

Analysis of Monkey Studies

PET studies were performed on three cynomolgus macaques (weight 6.9 ± 2.1 kg) with the multiple-injection approach. One animal (monN) was a healthy monkey aged 5 years, and the others had a syndrome acquired Parkinsonism. Of these, one (monUP, aged 7 years) had hemiparkinsonism induced by injecting the selective neurotoxin, *N*-methyl-4-pheny1-1,2,3,6-tetrahydropyridine (MPTP) (0.4 mg/kg) into the right carotid artery (Bankiewicz *et al*, 1986), whereas the other (monBP, aged 5 years) had bilateral Parkinsonism induced by injecting MPTP (0.4 mg/kg) intravenously and intermittently (twice a week for a total of 14 injections) (Takagi *et al*, 2005). Each Parkinsonian animal showed typical Parkinsonian symptoms in the limbs (motor slowness, tremor) unilaterally or bilaterally. The PET scan was performed after the symptom reaching stable (6 months after the first injection of MPTP). Anesthesia was induced with ketamine (8.4 mg/kg, intramuscularly) and xylazine (1.7 mg/kg, intramuscularly) and maintained by intravenous propofol (6 mg/kg/h) and vecuronium (0.02 mg/kg/h) during the scan. The monkeys were maintained and handled in accordance with guidelines for animal research on Human Care and Use of Laboratory Animals (Rockville, National Institutes of Health/Office for Protection from Research Risks, 1996). The study protocol was approved by the Subcommittee for Laboratory Animal Welfare of the National Cardiovascular Center.

After the synthesis of [^{11}C]raclopride, nonradioactive raclopride was added so that targeted molar amount of raclopride would be administered for three injections (1.5, 10, and 30 nmol/kg); this was done by dividing the [^{11}C]raclopride diluted by nonradioactive raclopride into three portions with different volumes, containing the intended masses of raclopride. For the first injection, 1.9 ± 0.16 nmol/kg (57.0 ± 5.7 MBq) of [^{11}C]raclopride was administered by a bolus injection at the beginning of the scan. Fifty minutes later, the second [^{11}C]raclopride injection, 11.1 ± 0.56 nmol/kg (60.4 ± 8.8 MBq at the time of second injection) was administered by a bolus, and 50 mins after that, a bolus of 31.1 ± 2.1 nmol/kg (30.8 ± 4.4 MBq at the time of third injection) of [^{11}C]raclopride was administered again. Data were acquired for 150 mins (10 secs × 18, 30 secs × 6, 120 secs × 7, 300 secs × 6; total 50 mins for each injection). The specific radioactivity was 4.7 ± 2.2 GBq/μmol at the time of the first injection.

PET scans were performed using a PCA-2000A positron scanner (Toshiba Medical Systems Corporation, Otawara, Japan) that provides 47 planes and a 16.2 cm axial field-of-view. The transaxial and axial spatial resolution of the PET scanner were 6.3 and 4.7 mm full width at half maximum (Herzog *et al*, 2004). A transmission scan with a 3-rod source of ^{68}Ge-^{68}Ga was performed for 20 mins for attenuation correction before the administration of [^{11}C]raclopride. Radioactivity was measured in the three-dimensional mode and the data were reconstructed by a filtered back-projection using a Gaussian filter (3 mm of full width at half maximum). Region-of-interests (ROIs) were defined manually over the left and right striatum and cerebellum for PET images, and the radioactivity concentrations in these regions were obtained. For the left and right striatum, R_1, k_2, and BP_{ND} for each injection were estimated by the MI-SRTM. In addition, parametric images were generated, estimating each parameter voxel by voxel, using the MI-SRTM with a basis function method in which the model Equation (1) was solved using linear least squares for a set of basis functions, which enables the incorporation of parameter bounds (Gunn *et al*, 1997; Ikoma *et al*, 2009). B_{max} and K_d were estimated by the MI-GA from these BP_{ND} values of left and right striatum for three injections.

In the unilateral Parkinsonian animal, three PET scans with conventional single injection with different masses of [^{11}C]raclopride were also performed for comparison with results by the multiple-injection single PET scan approach. A PET scan with a bolus injection of 2.1 nmol/kg (50.6 MBq), 11.3 nmol/kg (60.4 MBq), or 31.1 nmol/kg (30.8 MBq) of [^{11}C]raclopride was obtained on separate days. PET data were acquired for 50 mins with the same protocol as the single PET scan approach. The values of R_1, k_2, and BP_{ND} were estimated by the SRTM, and B_{max} and K_d were estimated by the conventional graphical analysis.

Results

Simulation Study

Effect of Injected Mass on BP_{ND} Estimates: In the simulations, the value of BP_{ND}, estimated by the MI-SRTM, decreased as injected molar amount of raclopride increased, that is, concentration of bound raclopride became larger. The relationship between BP_{ND} and B^{ref} had a good linear correlation to some extent; however, it did not remain linear for large B^{ref} (Figure 2A). The regression line where $B^{ref} < 20$ pmol/mL was $BP_{ND} = -0.091B^{ref} + 2.4$, $R^2 = 0.997$ for the first injection. In the relationship between BP_{ND} and B^{ref}, BP_{ND} values of the third injection were higher than those of the first injection when B^{ref} was lower than 20 pmol/mL. The ratio B^{ref}/F^{ref} was almost the same as the BP_{ND} estimated by MI-SRTM, though it was a little smaller when B^{ref} was lower than 5 pmol/mL (Figure 2B).

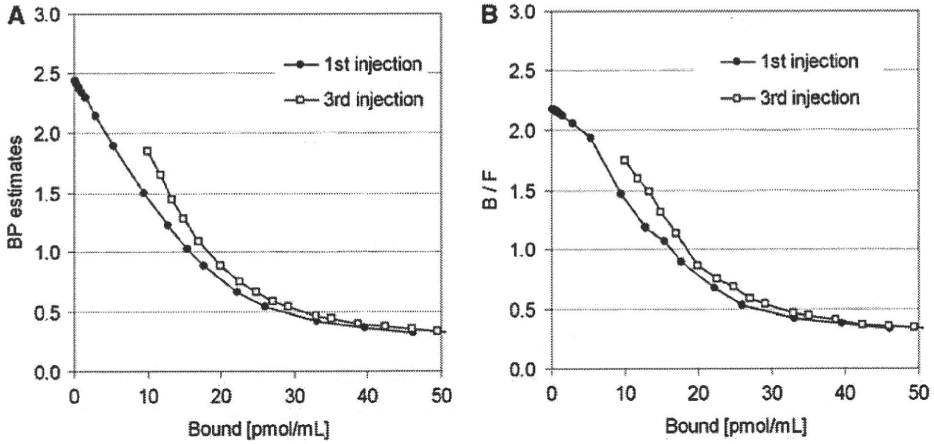

Figure 2 Relationship between specifically bound concentration and BP_{ND} (**A**) or B^{ref}/F^{ref} (**B**) estimates for the first and third injection in the simulations.

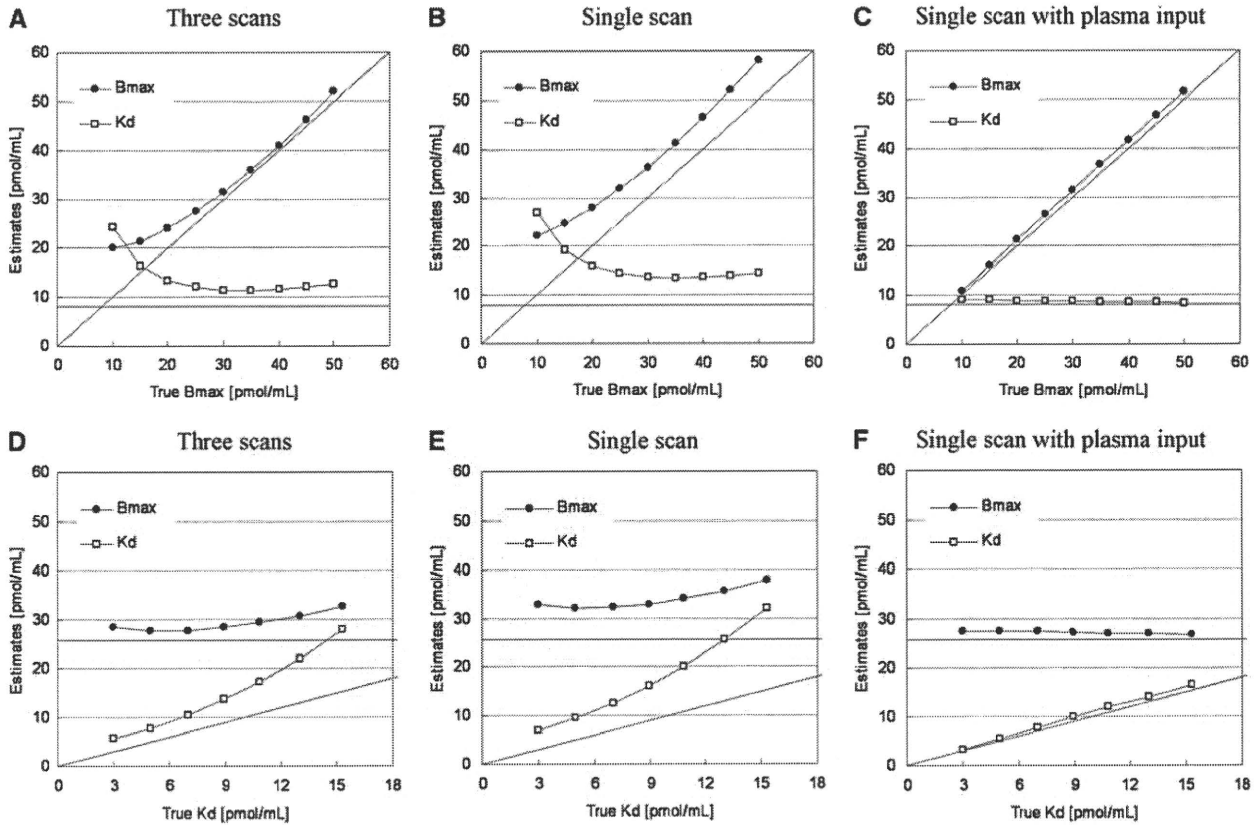

Figure 3 Relationships between estimates and true values of B_{max} and K_d for simulated TACs with various B_{max} and fixed K_d (**A–C**) and with various K_d and fixed B_{max} (**D–F**) by the three PET scan approach (**A**, **D**), multiple-injection single PET scan approach (**B**, **E**), and single PET scan approach with the plasma input function (**C**, **F**).

Estimation of B_{max} and K_d Values by the Multiple-Injection Graphical Analysis: The TACs were calculated for a range of possible B_{max} and K_d values, and the relationship between true and estimated B_{max} or K_d values was investigated for conventional three PET scan and the proposed single PET scan approaches. When B_{max} was varied, B_{max} and K_d were overestimated compared with the true values in both three PET scan and single PET scan approaches (Figures 3A and 3B). However, a good correlation was observed between true and estimated B_{max}, and there was little variation in estimated K_d when B_{max} was set higher than 20 pmol/mL. Similarly, when K_d was varied, although K_d and B_{max} were overestimated in both approaches, there was a good correlation between true and estimated K_d, and estimated B_{max} was constant (Figures 3D and 3E). In both cases, B_{max} and K_d estimates in the single

PET scan approach were higher than those in the three PET scan approach. In the TAC simulated with $B_{max} = 25.7$ and $K_d = 7.0$, estimated B_{max} and K_d were 27.8 and 10.5, respectively, in the three PET scan approach, and 32.3 and 12.6, respectively, in the single PET scan approach. In contrast to these approaches with the reference TAC, the overestimation of B_{max} and K_d was scarcely observed in the MI-GA with the plasma input function (Figures 3C and 3F).

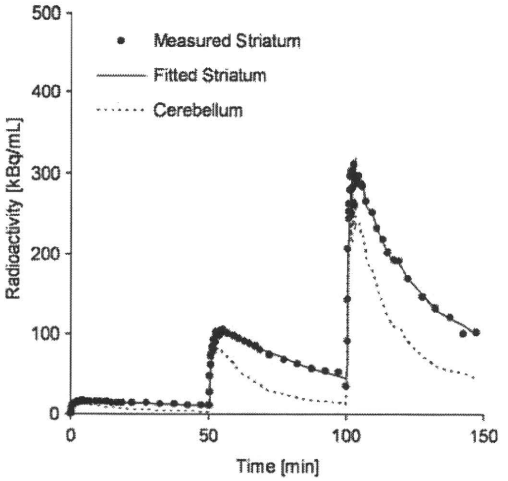

Figure 4 Measured TACs of the striatum and cerebellum and a fitted curve for the striatum using MI-SRTM in the monkey study by a single scan with sequential three injections of [^{11}C]raclopride.

Monkey Studies

Typical examples of TACs for the striatum and the cerebellum in the multiple-injection study are shown in Figure 4, and the parametric images of BP_{ND} for the first, second, and third injection, and images of B_{max} and K_d for the voxels in which BP_{ND1} was higher than 1.5 are shown in Figure 5. The estimated BP_{ND} decreased as the injected molar amount of [^{11}C]raclopride became larger in the second or third injection. Estimated BP_{ND1}, BP_{ND2}, and BP_{ND3} values were 2.3, 1.4, and 0.74, respectively, in the left striatum, and 2.6, 1.9, and 0.87, respectively, in the right striatum. The reduction in BP_{ND} was also observed in the parametric images.

The plots of MI-GA are shown in Figure 6. Plots of MI-GA for each of three animals were on the line, and B_{max} and K_d could be estimated as summarized in Table 1. Using the single scan approach for the hemiparkinsonian animal, B_{max} was 42.3 pmol/mL and K_d was 15.2 pmol/mL in the affected (right) striatum, and B_{max} was 32.3 pmol/mL and K_d was 13.0 pmol/mL in the contralateral (left) normal striatum. Corresponding estimates for the three scan approach were $B_{max} = 36.4$ and $K_d = 13.3$ pmol/mL in the right striatum and $B_{max} = 29.2$ and $K_d = 11.6$ pmol/mL in the

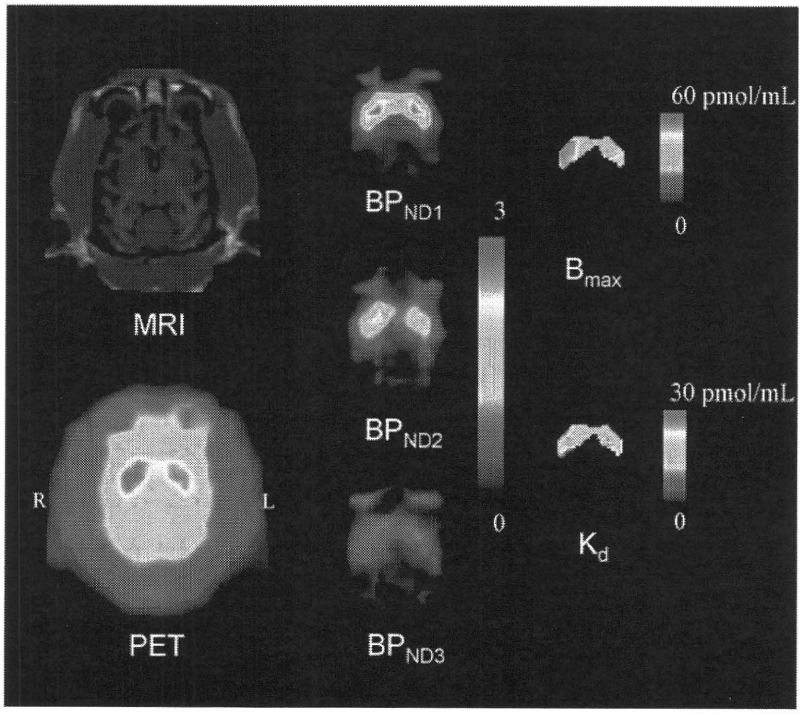

Figure 5 MRI and PET summation image (left) and parametric images of BP_{ND} for the first, second, and third injection (center) and parametric images of B_{max} and K_d for the voxels in which BP_{ND1} is higher than 1.5 (right) in the unilateral Parkinsonian (monUP) monkey study by a single scan with three sequential injections of [^{11}C]raclopride. Although ROI analysis disclosed higher B_{max} values in the MPTP-infused side of the striatum, the parametric image showed more evident increase of B_{max} in the dorsal and posterior parts of the striatum.

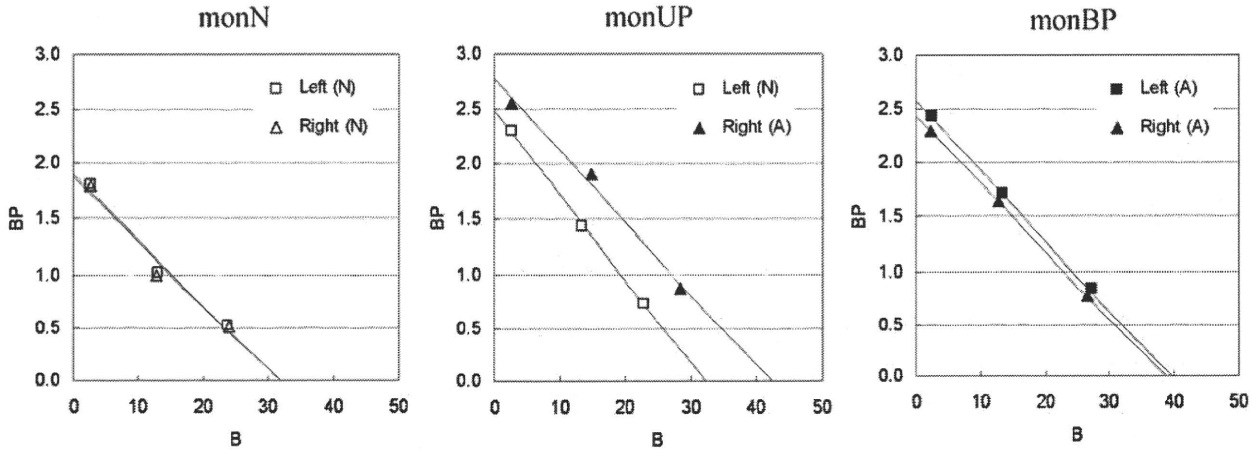

Figure 6 Single-scan, multiple-injection graphical analysis for normal (N) or affected (A) region of the left or right striatum in three monkeys that were normal (monN), unilateral Parkinsonian (monUP), and bilateral Parkinsonian (monBP).

Table 1 Estimated B_{max} and K_d values in three monkey studies

Scan protocol	*Subject*	*Region*	*Diagnosis*	B_{max} *(pmol/mL)*	K_d *(pmol/mL)*
Single scan	monN	L	N	31.8	16.7
		R	N	31.7	16.9
	monUP	L	N	32.3	13.0
		R	A	42.3	15.2
	monBP	L	A	39.6	15.4
		R	A	38.7	15.9
Three scans	monUP	L	N	29.2	11.6
		R	A	36.4	13.3

L, left striatum; R, right striatum; N, normal striatum; A, affected striatum.

left striatum. Both B_{max} and K_d of the single PET scan approach were slightly higher than those of the three PET scan approach. However, importantly, both approaches found that B_{max} in the affected striatum was higher than that in the normal striatum. The bilateral Parkinsonian animal showed B_{max} values of left = 39.6 pmol/mL, right = 38.7 pmol/mL, both of which were higher than those of the striatum of the normal animal or the normal striatum of the unilateral animal, but were very close to the affected striatum of the unilateral animal. The K_d values of the bilateral animal were not so different from other striatums.

Discussion

Density and Affinity Determination by Graphical Analysis with the Reference Region

In the graphical analysis for PET receptor studies, the values of B_{max} and K_d were estimated from the relationship between the ratio of bound to free concentrations and bound concentration at the time of transient equilibrium, using the TAC of the reference region (Farde *et al*, 1986). Some groups have used the value estimated from the distribution volume ratio − 1, instead of the B^{ref}/F^{ref} value of the y axis, because the values of B^{ref}/F^{ref} could change considerably with small changes in the time point of the transient equilibrium T_{eq} determined as the maximum C_b^{ref} (Logan *et al*, 1997; Doudet and Holden, 2003; Doudet *et al*, 2003). Distribution volume ratio or BP_{ND} is estimated from the kinetic analysis with TACs of target and reference regions, so it is not affected by the error of estimated T_{eq}. On the other hand, the value of $k'_3(t)$ in Equation (2) varies according to the concentration of bound raclopride, and estimates of BP_{ND} are considered to be an averaged value of specific binding over time, which is influenced by the dynamics of the free and bound raclopride. Despite this, in our simulation study of [^{11}C]raclopride, there was little difference between B^{ref}/F^{ref} and BP_{ND} estimated by the SRTM, and both had a linear correlation with B^{ref} (Figure 2). However, B^{ref}/F^{ref} became smaller than BP_{ND} and deviated from the linear relationship between B^{ref}/F^{ref} and B^{ref} in the region with low B^{ref} (Figure 2), especially for the TACs with high B_{max}. This may be a result of imperfect attainment of the transient equilibrium within the 50 mins scan duration for the TAC with high binding. There was little effect of the error of B^{ref} for the graphical analysis, in which B^{ref} varied widely among three injections, whereas the error of B^{ref}/F^{ref}

because of nonachievement of transient equilibrium had much effect on the graphical analysis as compared with BP_{ND}. Therefore, we estimated B_{max} and K_d by the graphical analysis with the relationship between BP_{ND} and B^{ref}.

In the simulations with various injected masses of [^{11}C]raclopride, it was shown that the relationship between BP_{ND} and B^{ref} became linear to some extent. However, BP_{ND} deviated from the linear relationship and approached a nonzero value when B^{ref} became larger (Figure 2). Therefore, in the B_{max} and K_d estimation by the graphical analysis with the reference TAC, points must be plotted within the range of the linear relation. As the relationship between BP_{ND} and B estimated from C_b using the plasma input function, without the reference TAC, remained linear even when B became large and the estimated BP_{ND} approached 0 (data not shown), this apparent saturation seemed to be owing to the reference region. Strictly speaking, the time course of free radioligand C_f is different from that of the reference region C_r (Figure 1) and C_f changes according to the specific binding that was affected by k_{on}, B_{max}, or administered mass of raclopride as pointed out by Ito *et al* (1998). Therefore, the time of the transient equilibrium estimated using C_b^{ref} was different from that estimated using C_b, and B^{ref} was often different as well. In addition, the value of BP_{ND} estimated by SRTM was lower than the BP_{ND} estimated from the two-tissue compartment model with the plasma input function.

This difference between the target and reference TAC affected the B_{max} and K_d estimates as well. In the simulated TACs with various B_{max} or K_d values, the B_{max} and K_d were overestimated compared with the true values even in the conventional three PET scan approach (Figure 3). On the other hand, the overestimation was not observed when B_{max} and K_d were estimated by the graphical analysis using C_f and C_b without the reference TAC (Figure 3), demonstrating that graphical analysis could determine B_{max} and K_d precisely if C_b were obtained correctly. However, the free and bound concentrations in the target region cannot be distinguished from the total concentration measured by PET scanning without arterial blood sampling, and in practical PET data, estimation of rate constants with the plasma input function is unstable and impractical. Therefore, in the usual graphical analysis, the TAC of reference region is used as the free radioligand concentration in the target region (Farde *et al*, 1989). The effect of the reference TAC on B_{max} and K_d estimates depends on the kinetics of the tracer in each region, which depends in turn on the particular tracers and species. In the simulated TACs of monkeys with [^{11}C]raclopride, there was a good correlation between true and estimated K_d or B_{max}, though estimates were biased. Therefore, we concluded the graphical analysis with reference TAC is practical for [^{11}C]raclopride studies, because it can detect the value of B_{max} or K_d in neurological or psychiatric disorders without arterial blood sampling.

Estimated Density and Affinity by the Multiple-Injection Approach

We applied the multiple-injection approach to the graphical analysis for B_{max} and K_d determination in an effort to shorten the total duration of the scanning protocol, and to obviate the need for several radiosyntheses for each animal. From the relationship between the BP_{ND} estimates and injected mass in the simulation study (Figure 2), the molar amounts of three injections were set as 1.5, 10, and 30 nmol/kg, so that the estimated BP_{ND} would be high, intermediate, and low within the range in which the linear correlation held. The injection interval was set to 50 mins, because it has been reported in monkey studies that 50 mins scan duration could provide reliable BP_{ND} estimates even for TACs with high and low BP_{ND} values (Ikoma *et al*, 2009). In our present studies on monkeys with this protocol, injected masses increased with each successive injection, but amounts of administered radioactivity remained fairly constant, i.e., 57, 60, and 31 MBq. Therefore, the signal to noise ratio of image quality did not change seriously for each injection.

In the usual graphical analysis by nonsequential multiple PET scans, the molar amount of administered [^{11}C]raclopride for each scan is adjusted by varying the specific activity of administered [^{11}C]raclopride. Several investigators have attempted to perform multiple injections of ligands with PET studies to obtain receptor density and affinity by changing specific activity with a detailed model equation (Delforge *et al*, 1995; Millet *et al*, 1995; Morris *et al*, 1996; Muzic *et al*, 1996; Christian *et al*, 2004; Gallezot *et al*, 2008). Meanwhile, our approach requires only one synthesis of [^{11}C]raclopride, which is split to three with different mass of raclopride with same specific activity. By keeping the specific activity throughout scan, we can directly interpret PET counts in pmol/mL unit.

In the simulations of B_{max} and K_d estimation with this single PET scan approach, B_{max} and K_d were overestimated compared with the true values, just as seen in the three PET scan approach. Furthermore, estimates of both parameters were higher than those in the three PET scan approach. In the single PET scan approach, the error because of assumptions of the reference tissue approach could be more severe than for the three PET scan approach, because the residual radioactivities at the times of the second and third injections could propagate to error of B^{ref} or BP_{ND} estimates. This was shown to be the case in the simulation study, in which the relationship between the BP_{ND} and B^{ref} in the third injection was a little different from that in the first injection (Figure 2). Furthermore, our approach assumes that BP_{ND} is promptly altered by the next injection, but this is in fact not exactly the case. We showed the bias of the estimated BP_{ND} related to this assumption (Ikoma *et al*, 2009), and the estimated B_{max} and K_d in this paper consequently could be biased. However, in the

simulations, B_{max} and K_d estimated by the MI-GA changed according to the variation of the true values (Figure 3), demonstrating this approach could be applied to the quantitative evaluation of B_{max} and K_d from a single session of PET scanning.

Monkey Studies

In the simulations, we demonstrated that the MI-GA could detect density and affinity of dopamine D_2 receptors. Furthermore, we demonstrated the validity of the proposed method using actual data from monkeys. As a result, the three BP_{ND} data points calculated from the single PET scan with three sequential injections of different administration masses were almost on a straight line, and estimated values of B_{max} and K_d were very close to those previously obtained *in vitro* ($B_{max} = 25.7$ pmol/g) (Madras *et al*, 1988) or *in vivo* by the conventional method in monkeys ($B_{max} = 22$ pmol/mL, $K_d = 13.5$ nmol/L) (Doudet *et al*, 2003). The estimates by the single PET scan approach were slightly higher than those by the three PET scan approach, and this was consistent with the results from the current simulations.

Although we investigated only three monkeys in this study, the values of B_{max} in the partially denervated striata was higher than in normal striatum, whereas the apparent affinity was unaffected by the MPTP lesions. Likewise Rinne *et al* (1995) reported a 35% increase in the D_2 B_{max} in the putamen contralateral to the side of predominant motor symptoms, without any discernible effect on apparent affinity. In our monkey measurements, in the hemilesioned monkey, the B_{max} was elevated by 31% on the denervated side. In the animal with bilateral MPTP lesion, the B_{max} in both striata was higher than in the normal animal, or in the unlesioned side of the hemiparkinsonian animal, despite no significant changes in K_d values: the results were consistent with those of the previous report.

In addition to the results of ROI analysis, which disclosed bulk D_2 receptor characteristics in the whole striatum, parametric imaging of B_{max} and K_d (as shown in Figure 5) suggested a potential significance in regional estimation of D_2 receptor characteristics. Although ROI analysis disclosed higher B_{max} values in the MPTP-infused side of the striatum, the parametric imaging showed the increase of B_{max} was more evident in the dorsal and posterior parts of the striatum. A similar finding of preferential lesion in dorsal and posterior parts of the striatum has been reported based on neurochemical and pathological assessments of MPTP-lesioned monkeys (Oiwa *et al*, 2003). As the current parametric imaging may have significant artifacts, such as those arising from low signal-to-noise ratio, partial volume effects, small number of points, the situation should be improved through the use of a higher resolution PET scanner.

Potential Limitations of the Multiple-Injection Graphical Analysis

The multiple-injection approach is able to assess the B_{max} and K_d for receptor studies in a single PET scan with single radiosynthesis, and shortened study period as compared with a conventional approach. This approach might also be applicable to other PET ligands and receptor types, but with several caveats: First, it is necessary to evaluate whether the reference region can be used as the free TAC of the target region. The kinetics of the target and reference regions is affected by the value of each rate constant, i.e., K_1, k_2, B_{max}, and K_d, that differ between species and radioligands. The difference between C_{ref} and C_f often causes an error in B^{ref}, and the estimated B_{max} and K_d should be interpreted with caution when the reference region has considerably different kinetics. Second, the molar amounts of administered ligand need to be selected such that the resultant BP_{ND} will be within the range in which the linear relationship between BP_{ND} and B holds. In the case of regions with low BP_{ND}, and small extent of the necessary linear relationship, it may be difficult to determine B_{max} and K_d reliably. Third, the interval of three injections should be determined so that the free ligand TAC has a transient equilibrium within the scan duration of each injection, especially when the injected mass is small, i.e., BP_{ND} is high. The radioligand [^{11}C]raclopride dissociates rapidly from the receptors, allowing equilibration of binding to be established *in vivo* within the time span of PET experiments (Farde *et al*, 1989; Ito *et al*, 1998). However, those ligands with slow kinetics, such as [^{18}F]fallypride require a longer scan duration such that the present graphical analysis may not be suitable in all instances. Despite these limitations, by optimizing the administered mass and the time interval between three injections of [^{11}C]raclopride, we have shown that the multiple-injection approach can determine B_{max} and K_d values as effectively as an approach using three separate scans, but within a single scan time of 150 mins.

Moreover, the bias of B_{max} and K_d estimated by the single scan approach with two injections was not larger than that by the single scan approach with three injections in the simulations (data not shown), and points of the second and third injections in MI-GA were almost on the same line in the monkey studies (Figure 6). Therefore, there is a possibility of reducing scan time and exposure further using only two injections, though the effect of statistical noise on estimates should be considered.

Conclusion

We developed the method for estimating B_{max} and K_d values in a single session of PET scanning with multiple injections of [^{11}C]raclopride. Our simulations showed that the MI-GA could detect B_{max} and K_d values by using the optimal injection protocol. We

also demonstrated in monkey studies that B_{max} and K_d values estimated by our proposed approach were proper compared with previous monkey studies or our studies by the conventional method. The proposed method made it possible to determine the dopamine D_2 receptor density and affinity by a 150 mins PET scan with three injections of [^{11}C]raclopride at 50 mins intervals.

Acknowledgements

We thank Dr Jun Takahashi (Kyoto University) for providing us animals for this study. This research was supported by the Ministry of Education, Culture, Sports, Science and Technology of Japan (MEXT) grant-in-aid for Young Scientists (B) (No. 20790839), grant-in-aid for Scientific Research (C) (No. 09019855) (TH), Kobe Cluster I and II, and the Ministry of Health, Labour, and Welfare of Japan (MHLW) Health Science Research Grant, H17-025 (TH, HI). We are grateful to members of Department of Investigative Radiology, National Cardiovascular Center Research Institute, for their support of PET experiment and for helpful suggestions.

Conflict of interest

The authors declare no conflict of interest.

References

Bankiewicz KS, Oldfield EH, Chiueh CC, Doppman JL, Jacobowitz DM, Kopin IJ (1986) Hemiparkinsonism in monkeys after unilateral internal carotid artery infusion of 1-methyl-4-phenyl-1,2,3,6-tetrahydropyridine (MPTP). *Life Sci* 39:7–16

Christian BT, Narayanan T, Shi B, Morris ED, Mantil J, Mukherjee J (2004) Measuring the *in vivo* binding parameters of [^{18}F]-fallypride in monkeys using a PET multiple-injection protocol. *J Cereb Blood Flow Metab* 24:309–22

Cross AJ, Crow TJ, Owen F (1981) ^{3}H-Flupenthixol binding in post-mortem brains of schizophrenics: evidence for a selective increase in dopamine D2 receptors. *Psychopharmacology (Berl)* 74:122–4

Delforge J, Pappata S, Millet P, Samson Y, Bendriem B, Jobert A, Crouzel C, Syrota A (1995) Quantification of benzodiazepine receptors in human brain using PET, [^{11}C]flumazenil, and a single-experiment protocol. *J Cereb Blood Flow Metab* 15:284–300

Doudet DJ, Holden JE (2003) Sequential versus nonsequential measurement of density and affinity of dopamine D_2 receptors with [^{11}C]raclopride: Effect of methamphetamine. *J Cereb Blood Flow Metab* 23:1489–94

Doudet DJ, Jivan S, Holden JE (2003) *In vivo* measurement of receptor density and affinity: comparison of the routine sequential method with a nonsequential method in studies of dopamine D_2 receptors with [^{11}C]raclopride. *J Cereb Blood Flow Metab* 23:280–4

Farde L, Ehrin E, Eriksson L, Greitz T, Hall H, Hedström CG, Litton JE, Sedvall G (1985) Substituted benzamides as ligands for visualization of dopamine receptor binding in the human brain by positron emission tomography. *Proc Natl Acad Sci USA* 82:3863–7

Farde L, Eriksson L, Blomquist G, Halldin C (1989) Kinetic analysis of central [^{11}C]raclopride binding to D_2-dopamine receptors studied by PET — A comparison to equilibrium analysis. *J Cereb Blood Flow Metab* 9: 696–708

Farde L, Hall H, Ehrin E, Sedvall G (1986) Quantitative analysis of D_2 dopamine receptor binding in the living human brain by PET. *Science* 231:258–61

Farde L, Wiesel FA, Hall H, Halldin C, Stone-Elander S, Sedvall G (1987) No D_2 receptor increase in PET study of schizophrenia. *Arch Gen Psychiatry* 44:671–2

Farde L, Wiesel FA, Stone-Elander S, Halldin C, Nordström AL, Hall H, Sedvall G (1990) D_2 dopamine receptors in neuroleptic-naive schizophrenic patients. A positron emission tomography study with [^{11}C]raclopride. *Arch Gen Psychiatry* 47:213–9

Gallezot JD, Bottlaender MA, Delforge J, Valette H, Saba W, Dollé F, Coulon CM, Ottaviani MP, Hinnen F, Syrota A, Grégoire MC (2008) Quantification of cerebral nicotinic acetylcholine receptors by PET using 2-[^{18}F]fluoro-A-85380 and the multiinjection approach. *J Cereb Blood Flow Metab* 28:172–89

Gunn RN, Lammertsma AA, Hume SP, Cunningham VJ (1997) Parametric imaging of ligand-receptor binding in PET using a simplified reference region model. *Neuroimage* 6:279–87

Guttman M, Seeman P (1985) L-dopa reverses the elevated density of D_2 dopamine receptors in Parkinson's diseased striatum. *J Neural Transm* 64:93–103

Hall H, Köhler C, Gawell L, Farde L, Sedvall G (1988) Raclopride, a new selective ligand for the dopamine-D_2 receptors. *Prog Neuropsychopharmacol Biol Psychiatry* 12:559–68

Herzog H, Tellmann L, Hocke C, Pietrzyk U, Casey ME, Kuwert T (2004) NEMA NU2-2001 guided performance evaluation of four Siemens ECAT PET scanners. *IEEE Trans Nucl Science* 51:2662–9

Ikoma Y, Watabe H, Hayashi T, Miyake Y, Teramoto N, Minato K, Iida H (2009) Quantitative evaluation of changes in binding potential with a simplified reference tissue model and multiple injections of [^{11}C]raclopride. *Neuroimage* 47:1639–48

Ito H, Hietala J, Blomqvist G, Halldin C, Farde L (1998) Comparison of the transient equilibrium and continuous infusion method for quantitative PET analysis of [^{11}C]raclopride binding. *J Cereb Blood Flow Metab* 18:941–50

Joyce JN, Lexow N, Bird E, Winokur A (1988) Organization of dopamine D_1 and D_2 receptors in human striatum: receptor autoradiographic studies in Huntington's disease and schizophrenia. *Synapse* 2:546–57

Köhler C, Hall H, Ogren SO, Gawell L (1985) Specific *in vitro* and *in vivo* binding of ^{3}H-raclopride. A potent substituted benzamide drug with high affinity for dopamine D-2 receptors in the rat brain. *Biochem Pharmacol* 34:2251–9

Lammertsma AA, Hume SP (1996) Simplified reference tissue model for PET receptor studies. *Neuroimage* 4:153–8

Logan J, Fowler JS, Volkow ND, Wang GJ, Ding YS, Alexoff DL (1996) Distribution volume ratios without blood sampling from graphical analysis of PET data. *J Cereb Blood Flow Metab* 16:834–40

Logan J, Volkow ND, Fowler JS, Wang GJ, Fischman MW, Foltin RW, Abumard NN, Vitkun S, Gatley SJ, Pappas N, Hitzemann R, Shea CE (1997) Concentration and occupancy of dopamine transporters in cocaine abusers with [^{11}C]cocaine and PET. *Synapse* 27:347–56

Madras BK, Fahey MA, Canfield DR, Spealman RD (1988) D1 and D2 dopamine receptors in caudate-putamen of nonhuman primates (*macaca fascicularis*). *J Neurochem* 51:934–43

Millet P, Delforge J, Mauguiere F, Pappata S, Cinotti L, Frouin V, Samson Y, Bendriem B, Syrota A (1995) Parameter and index images of benzodiazepine receptor concentration in the brain. *J Nucl Med* 36:1462–71

Mintun MA, Raichle ME, Kilbourn MR, Wooten GF, Welch MJ (1984) A Quantitative model for the *in vivo* assessment of drug binding sites with positron emission tomography. *Ann Neurol* 15:217–27

Morris ED, Babich JW, Alpert NM, Bonab AA, Livni E, Weise S, Hsu H, Christian BT, Madras BK, Fischman AJ (1996) Quantification of dopamine transporter density in monkeys by dynamic PET imaging of multiple injections of ^{11}C-CFT. *Synapse* 24:262–72

Muzic RR, Nelson AD, Saidel GM, Miraldi F (1996) Optimal experiment design for PET quantification of receptor concentration. *IEEE Trans Med Imaging* 15:2–12

Oiwa Y, Eberling JL, Nagy D, Pivirotto P, Emborg ME, Bankiewicz KS (2003) Overlesioned hemiparkinsonian non human primate model: correlation between clinical, neurochemical and histochemical changes. *Front Biosci* 8:155–66

Rinne JO, Laihinen A, Ruottinen H, Ruotsalainen U, Någren K, Lehikoinen P, Oikonen V, Rinne UK (1995) Increased density of dopamine D_2 receptors in the putamen, but not in the caudate nucleus in early Parkinson's disease: a PET study with [^{11}C]raclopride. *J Neurol Sci* 132:156–61

Scatchard G (1949) The attractions of proteins for small molecules and ions. *Ann NY Acad Sci* 51:660–72

Seeman P, Bzowej NH, Guan HC, Bergeron C, Reynolds GP, Bird ED, Riederer P, Jellinger K, Tourtellotte WW (1987) Human brain D_1 and D_2 dopamine receptors in schizophrenia, Alzheimer's, Parkinson's, and Huntington's diseases. *Neuropsychopharmacology* 1:5–15

Takagi Y, Takahashi J, Saiki H, Morizane A, Hayashi T, Kishi Y, Fukuda H, Okamoto Y, Koyanagi M, Ideguchi M, Hayashi H, Imazato T, Kawasaki H, Suemori H, Omachi S, Iida H, Itoh N, Nakatsuji N, Sasai Y, Hashimoto N (2005) Dopaminergic neurons generated from monkey embryonic stem cells function in a Parkinson primate model. *J Clin Invest* 115:102–9

Watabe H, Ohta Y, Teramoto N, Miyake Y, Kurokawa M, Yamamoto A, Ose Y, Hayashi T, Iida H (2006) A novel reference tissue approach for multiple injections of [C-11]Raclopride. *Neuroimage* 31:T73

Wong DF, Wagner Jr HN, Tune LE, Dannals RF, Pearlson GD, Links JM, Tamminga CA, Broussolle EP, Ravert HT, Wilson AA, Toung JK, Malat J, Williams JA, O'Tuama LA, Snyder SH, Kuhar MJ, Gjedde A (1986) Positron emission tomography reveals elevated D_2 dopamine receptors in drug-naive schizophrenics. *Science* 234:1558–63

Appendix

The multiple-injection two-tissue four-parameter compartment model is based on the following differential equations:

$$\frac{dC_f}{dt} = K_1 C_p(t) - (k_2 + k_3) C_f(t) + k_4 C_b(t) \qquad \text{(A1)}$$

$$\frac{dC_b}{dt} = k_3 C_f(t) - k_4 C_b(t) \qquad \text{(A2)}$$

where C_p is the radioactivity concentration of metabolite-corrected plasma, C_f and C_b are the concentrations of radioactivity for free and specifically bound ligand in tissue, respectively.

Equations (A1) and (A2) are solved with the radioactivity concentration of C_f and C_b at the time of injection, that is $C_f(0)$ and $C_b(0)$, then $C_f(t)$, $C_b(t)$ and total radioactivity concentration in tissue $C_t(t)$ are expressed as following equations:

$$\begin{aligned} C_f(t) = {} & \frac{K_1}{\alpha_2 - \alpha_1}\{(k_4 - \alpha_1)e^{-\alpha_1 t} - (k_4 - \alpha_2)e^{-\alpha_2 t}\} \otimes C_p(t) \\ & + \frac{1}{\alpha_2 - \alpha_1}\{(k_4 - \alpha_1)C_f(0) + k_4 C_b(0)\}e^{-\alpha_1 t} \\ & - \frac{1}{\alpha_2 - \alpha_1}\{(k_4 - \alpha_2)C_f(0) + k_4 C_b(0)\}e^{-\alpha_2 t} \end{aligned} \qquad \text{(A3)}$$

$$\begin{aligned} C_b(t) = {} & \frac{K_1 k_3}{\alpha_2 - \alpha_1}(e^{-\alpha_1 t} - e^{-\alpha_2 t}) \\ & \otimes C_p(t) + \frac{k_3}{\alpha_2 - \alpha_1}\left(C_f(0) + \frac{k_4}{k_4 - \alpha_1} C_b(0)\right)e^{-\alpha_1 t} \\ & - \frac{k_3}{\alpha_2 - \alpha_1}\left(C_f(0) + \frac{k_4}{k_4 - \alpha_2} C_b(0)\right)e^{-\alpha_2 t} \\ & + \left(\frac{k_3 k_4}{(k_4 - \alpha_1)(k_4 - \alpha_2)} + 1\right) C_b(0) e^{-k_4 t} \end{aligned} \qquad \text{(A4)}$$

$$\begin{aligned} C_t(t) = {} & \frac{K_1}{\alpha_2 - \alpha_1}\{(k_3 + k_4 - \alpha_1)e^{-\alpha_1 t} - (k_3 + k_4 - \alpha_2)e^{-\alpha_2 t}\} \\ & \otimes C_p(t) + \frac{k_3 + k_4 - \alpha_1}{\alpha_2 - \alpha_1}\left(C_f(0) + \frac{k_4}{k_4 - \alpha_1} C_b(0)\right)e^{-\alpha_1 t} \\ & - \frac{k_3 + k_4 - \alpha_2}{\alpha_2 - \alpha_1}\left(C_f(0) + \frac{k_4}{k_4 - \alpha_2} C_b(0)\right)e^{-\alpha_2 t} \\ & + \left(\frac{k_3 k_4}{(k_4 - \alpha_1)(k_4 - \alpha_2)} + 1\right) C_b(0) e^{-k_4 t} \\ \alpha_{1,2} = {} & \frac{(k_2 + k_3 + k_4) \mp \sqrt{(k_2 + k_3 + k_4)^2 - 4k_2 k_4}}{2} \end{aligned} \qquad \text{(A5)}$$

3-Tesla Magnetic Resonance Angiographic Assessment of a Tissue-Engineered Small-Caliber Vascular Graft Implanted in a Rat

Masashi Yamanami,[1,2] Akihide Yamamoto,[3,4] Hidehiro Iida,[3,4] Taiji Watanabe,[1,2] Keiichi Kanda,[2] Hitoshi Yaku,[2] Yasuhide Nakayama[1]

[1] Department of Bioengineering, Advanced Biomedical Engineering Center, National Cardiovascular Center Research Institute, Osaka, Japan

[2] Department of Cardiovascular Surgery, Kyoto Prefectural University of Medicine, Kyoto, Japan

[3] Department of Investigative Radiology, Advanced Biomedical Engineering Center, National Cardiovascular Center Research Institute, Osaka, Japan

[4] Department of Medical Physics and Engineering, Division of Health Sciences, Graduate School of Medicine, Osaka University, Osaka, Japan

Received 30 January 2009; revised 4 June 2009; accepted 15 July 2009
Published online 2 October 2009 in Wiley InterScience (www.interscience.wiley.com). DOI: 10.1002/jbm.b.31501

Abstract: In the development of small-caliber vascular grafts (diameter; less than 3 mm), animal implantation studies have been mostly performed by using rat abdominal aortas, and their certain patency must evaluate with sacrificing every observation periods, which is both labor-intensive and time-consuming when performing a large number of experiments. This study is the first to demonstrate the application of 3-Tesla contrast-free time-of-flight magnetic resonance angiography (TOF-MRA) in the continuous assessment of the status of a tissue-engineered vascular graft in rat. As a model graft, a single connective tubular tissue (diameter; 1.5 mm), prepared by embedding the silicone rod (diameter; 1.5 mm) into a subcutaneous pouch of a rat for 2 weeks an *in vivo* tissue-engineering, was used. The graft was implanted in the abdominal aorta (diameter; 1.3 mm) of the rat by end-to-end anastomosis. Repeated TOF-MRA imaging of the graft obtained over a 3-month follow-up period after implantation made it possible to evaluate the patency of the graft, both simply and noninvasively. It also permitted visualization of the connected abdominal aorta and renal and common iliac arteries having smaller caliber (diameter; less than 1 mm). In addition, the degree of the stenosis or aneurysm could also be detected. 3-Tesla MRA allowed the simplified and noninvasive assessment of the status on the vascular graft, including the formation of a stenosis or aneurysm, in the same rat at different times, which will be contributing to enhance the development of tissue-engineered vascular grafts even with small caliber. © 2009 Wiley Periodicals, Inc. J Biomed Mater Res Part B: Appl Biomater 92B: 156–160, 2010

Keywords: small-caliber vascular grafts; magnetic resonance angiography; animal implantation; biotube; tissue engineering

INTRODUCTION

Small-caliber arterial substitutes are needed for cardiac and peripheral revascularization procedures. For such small artery bypass grafting procedures, autologous arterial (e.g., internal thoracic artery and radial artery) or venous (e.g., saphenous vein) grafts still remain the most ideal vascular substitutes.[1,2] However, many patients do not have a vessel suitable for use owing to the poor quality, inadequate size or length, or previous harvest of such vessels. Moreover, a second surgical procedure is required to initially obtain the necessary vessel. Vascular prostheses, such as expanded polytetrafluoroethylene (ePTFE) and poly (ethylene terephthalate) (Dacron) grafts, have been used clinically for reconstructing arteries.[3] However, small-caliber (<6 mm) arterial substitutes have generally proved inadequate largely because of the formation of thromboses and intimal hyperplasia.[4,5]

Many design criteria have been proposed for the development of functional small-caliber arterial replacement grafts.[5–11] All most of all artificial vascular grafts (inner diameter, 1.5–3.0 mm) have been employed for transplantation

Correspondence to: Y. Nakayama (e-mail: nakayama@ri.ncvc.go.jp)

to rat abdominal aortas as an *in vivo* model.[6–8] Graft patency has been evaluated during the follow-up period by angiography[8] or by direct inspection at the time of removal for histological evaluation.[6,7] However, angiography requires cannulation of the carotid artery,[8] and a midline laparotomy is needed for direct inspection.[6,7] As a consequence, these methods are complex and invasive. Therefore, it is difficult to evaluate graft patency repeatedly in the same rat. Although, graft patency has also been evaluated by palpating the femoral pulse,[7] this method is subjective and uncertain.

The current imaging systems, including fluorescence antibody method, single photon emission computed tomography (SPECT),[12] laser doppler system,[13] or high-resolution ultrasound[14] for blood flow imaging in addition to magnetic resonance angiography (MRA), are powerful tool in tissue engineering field. However, it is considered that no imaging systems except for MRA fit for evaluation of the status of implanted small-caliber vascular grafts.

In clinical practice, MRI has been used as a noninvasive evaluation method for the assessment of brain blood vessels and peripheral arteries and also been widely used in preclinical research on experimental small rodents.[15–18] The studies have typically been aimed at understanding the patho-physiological status and evaluating the efficacy/side effects of newly developed treatments, such as pharmaceutical and regenerative medicine.

Our purpose in this study was to evaluate the status of a tissue-engineered vascular graft with inner diameter of 1.5 mm, clinically, repeatedly, and noninvasively in a rat implantation model. To this end, 3-Tesla contrast-free time-of-flight magnetic resonance angiography (TOF-MRA) was applied.

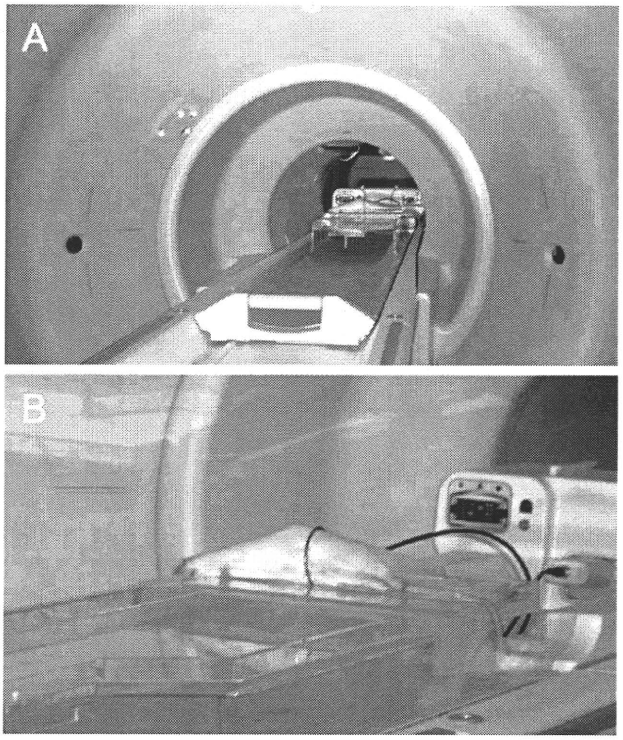

Figure 1. Experimental setup in MR imaging on a human whole-body 3T-MR scanner (GE Healthcare) (A). The coil was placed at the center of the gantry and its turn axis had perpendicular alignment to the static magnetic field (B). Rat's abdomen was positioned inside the coil along the craniocaudal direction. [Color figure can be viewed in the online issue, which is available at www.interscience.wiley.com.]

MATERIALS AND METHODS

Preparation and Implantation of the Connective Tubular Tissue

All animal experiments were conducted in accordance with local regulations, complying with the Principles of Laboratory Animal Care (formulated by the National Society for Medical Research) and the Guide for the Care and Use of Laboratory Animals (NIH Publication No. 86–23, revised 1985). The research protocol (No. 8050) was approved by the ethics committee of the National Cardiovascular Center Research Institute.

The connective tubular tissue was prepared by *in vivo* tissue engineering according to the previous reported method.[9] Briefly, a silicone rod (diameter, 1.5 mm; length, 10 mm; Tigers Polymer, Osaka, Japan) was used as a mold. One adult female Wistar rat (weight; 300 g) was anesthetized with 1.5% isoflurane (vol/vol air). The mold was placed in a dorsal subcutaneous pouch, and after 2 weeks, the implant was removed. The tubular tissue was obtained from the implant after trimming the peripheral tissues and pulling out the rod. The tube thus obtained was treated by coating with Argatroban (1 mg/graft; Mitsubishi Chemical Co., Tokyo, Japan) to make it antithrombogenic. It was then implanted to the infrarenal abdominal aorta of the same rat using an end-to-end anastomosis under microscopic guidance and sutured using 12 interrupted 10–0 nylon stitches [Figure 1(A)]. Patency was examined at the time of surgery by direct inspection. The wound was closed with 4–0 silk sutures. Thereafter, the rat had free access to standard food and water. Graft status was evaluated at 2, 36, and 78 days after transplantation by contrast-free TOF-MRA under anesthesia induced by an intramuscular injection of pentobarbital (40 mg/kg).

MR Data Acqusition

A human whole-body 3-Tesla magnetic resonance imaging (MRI) scanner (Signa, GE Healthcare, Milwaukee, WI) was employed in this study (Figure 1). The gradient coil system was capable of providing a maximum gradient amplitude of 40 mT/m. All sequence programs employed in this study were designed for clinical studies. A developed single-turn surface coil of 62 mm diameter was used for MR imaging [Figure 1(B)]. Contrast-free TOF-MRA was performed using a three-dimensional flow-compensated fast spoiled gradient recalled (3D-FSPGR) sequence [repetition

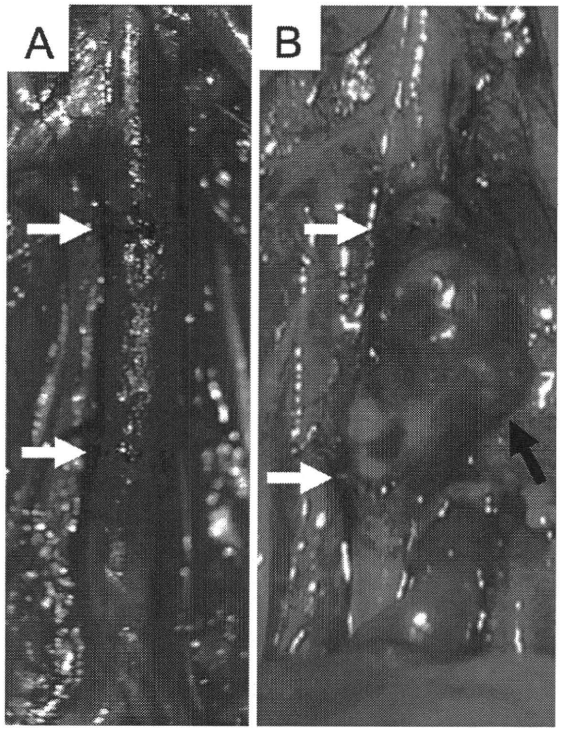

Figure 2. (A) The tubular connective tissue vascular graft (diameter; 1.5 mm) after autoimplantation in the rat infrarenal abdominal aorta (diameter; 1.3 mm) performed by end-to-end anastomosis under microscopic guidance using 12 interrupted stitches of 10-0 nylon suture. (B) The tubular connective tissue formed an aneurysm (max diameter; 3.0 mm) at 78 days after autoimplantation. White arrows indicate the proximal and distal anastomosis regions. Black arrow indicates the aneurysm. [Color figure can be viewed in the online issue, which is available at www.interscience.wiley.com.]

time (TR) = 21 ms, echo time (TE) = 5.4 ms (out of phase), flip angle (FA) = 15°, slice thickness = 0.4 mm, field of view (FOV) = 80 mm × 60 mm, matrix = 288 × 192, locs per slab = 128, the number of excitations (NEX) = 1, scanning time = 5 min 58 s]. For suppressing venous signals, a region of 40-mm thickness on the caudal side of the measured slab was saturated. The measured voxel size in TOF-MRA was 0.278 × 0.291 × 0.400 mm. The image reconstruction was zero-filled to a matrix size of 512 × 512 and the voxel size was 0.156 × 0.156 × 0.400 mm. MR angiograms were analyzed by generating the partial maximum intensity projection (pMIP) with a commercial software package (AZE, Tokyo, Japan). Our previous report on TOF-MRA was shown detail in rat.[13]

RESULTS

The tubular connective tissue with a diameter of 1.5 mm was autoimplanted successfully into the 1.3 mm diameter abdominal aorta of the rat by end-to-end anastomosis [Figure 2(A)]. After suturing with 12 interrupted stitches, there was little bleeding from either of the sites of anastomosis, indicated by the arrows in Figure 2(A). The patency of the graft was recognized directly by the satisfactory pulsation at the graft and distal side of the aorta.

3-Tesla contrast-free TOF-MRA of the rat was performed at 2 days after implantation [Figure 3(A)] to evaluate the status of the graft. The measurement time was ~6 min and no contrast medium was needed. The MRA distinctly visualized the patent graft connected to the abdominal aorta together with renal arteries and common iliac arteries of 0.7 and 0.8 mm diameter, respectively. Spatial resolution in the MRA was less than several hundred microns. A mechanical stenotic lesion, which may have been due to the anastomosis, was observed in both anastomosis regions. At 36 days after implantation, little stenosis and no aneurismal dilation of the graft were observed [Figure 3(B)]. At 78 days after implantation, the maximum diameter of the aneurysm formed at the graft was 3.0 mm [Figure 3(C)]. The shape of the aneurysm was very close to that observed macroscopically [Figure 2(B)]. Therefore, the status of the graft could be precisely determined, repeatedly, and noninvasively.

DISCUSSION

This study is the first to demonstrate the application of MRA to the evaluation of the status of a small-caliber arti-

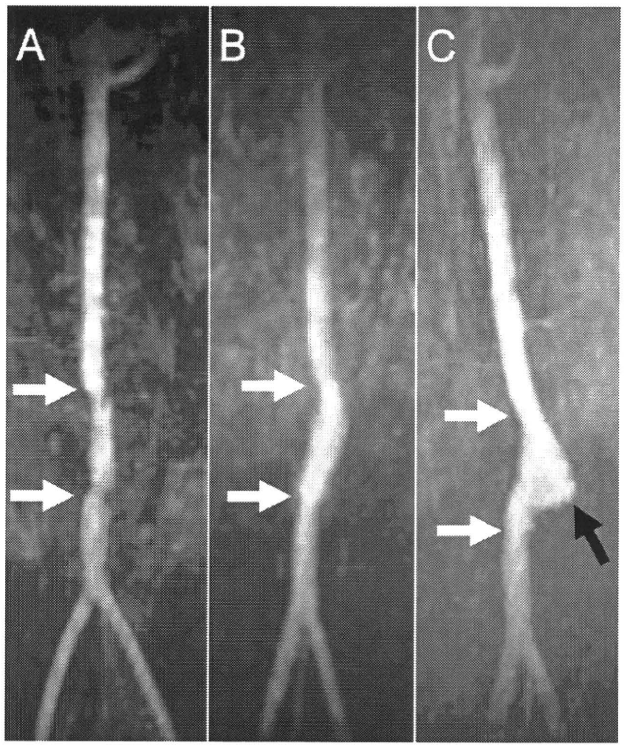

Figure 3. 3-Tesla contrast-free TOF-MRA images of the rat abdominal aorta at 2 (A), 36 (B), and 78 (C) days after autoimplantation of the biotube vascular graft. White arrows indicate the proximal and distal anastomosis regions of the abdominal aorta. A stenotic lesion was visible in the anastomosis regions at 2 days. An aneurysm formation in the graft was visible at 78 days (black arrow indicates the aneurysm).

ficial vascular graft implanted in the abdominal aorta of a rat. In the development of small-caliber vascular grafts as a preclinical study, *in vivo* evaluation is needed. Implantation studies have been performed mostly by using the abdominal aorta of rats.[6–8] Their certain patency must evaluate with sacrificing every observation periods, which is both labor-intensive and time-consuming when performing a large number of experiments. Since some rats survive with no symptoms after graft occlusion, assessment of the occlusion of an abdominal aorta after graft implantation is not possible solely on the basis of the rat's appearance. On the other hand, some researchers have evaluated graft patency by palpating the femoral pulse[7]; however, this method is prone to subjectivity and uncertainty. Therefore, evaluation of graft patency should be performed by direct inspection under laparotomy. On the other hand, even in histological observations, the evaluation of the degree of graft stenosis is very difficult.

In this study, MRI images of a reasonable quality were obtained from a rat using a human whole-body MRI scanner at 3-Tesla. Contrast-free TOF-MRA was able to depict the implanted graft with a diameter of ~1.5 mm, connected to the abdominal aorta with a diameter of ~1.3 mm, and also revealed arteries with diameters of less than 1 mm, such as the renal, common iliac, and tail arteries. In addition, an evaluation of the graft status, including the stenosis, was also feasible due to the high resolution and reasonable contrast. As indicated in Figure 3(A), the mechanical stenosis was clearly indicated at both sites of anastomosis. Furthermore, the aneurysm formation was clearly observed [Figure 3(C)]. Since the observation by MRA is simple and noninvasive, assessment of the status of small-caliber vascular grafts could be performed in the same rat at different times. The repeatable MRA observation in a single rat enabled correct assessment of the graft status over the follow-up period. Such repeatability will reduce the variation in results stemming from individual difference in experimental animals.

As a model graft for implantation in this study, the tubular connective tissue was used. The tissue was prepared similar to biotubes.[9] Biotubes are autologous prosthetic tubular tissues prepared by in-body tissue architecture technology. The biotube, obtained from rats by embedding the silicone rods (diameter; 3 mm) into their subcutaneous pouches for 4 weeks, had several 10 μm in thickness, about 500 gf in maximum load at rapture, and about 1000 mmHg in burst pressure.[19] This technology, a novel and practical concept in regenerative medicine, is based on the phenomenon of tissue encapsulation of foreign materials *in vivo*, and it can be used to develop autologous tissues of the desired shape, depending on the mold design.[9–11] Using this technology, several types of tissues, including "biotubes" as vascular tissues,[9–11] "biovalves" as tri-leaflet heart valve-shaped tissues,[20,21] and "biocovered stents" as hybrid IVR devices,[22] have been developed. In this study, by shortening of the encupsulation period weak and ununiform wall structure was prepared particularly for observation of the variety of vascular graft fate. As expected, normal, stenosis, or aneurysm models were appropriately obtained in one rat.

The assessment of graft status using MR imaging does, however, have limitations. When using certain materials for artificial grafts (e.g., ePTFE and Dacron), MR imaging might be difficult owing to graft artifacts. Furthermore, such as ultrasound and/or digital subtraction angiography, it is difficult to evaluate blood stream by 3D evaluation. The TOF-MRA is more appropriate for the evaluation of tissue-engineered vascular grafts. The signal-to-noise ratio in image quality on TOF-MRA is strongly dependent on the static field strength and the coil design. Further study should be needed in developing coil. We hope that others who study at understanding the patho-physiological status and evaluating the efficacy/side effects of newly developed treatments, such as pharmaceutical and regenerative medicine.

CONCLUSIONS

Contrast-free TOF-MRA with 3-Tesla allowed an assessment of tissue-engineered small-caliber vascular graft status in the rat systemic arterial circulation. As the protocol used in this study is simple and noninvasive, it is useful for the longitudinal evaluation of graft status in the rat; this will contribute to enhancing the development of tissue-engineered small-caliber vascular grafts, particularly in the field of regenerative medicine.

REFERENCES

1. Tomizawa Y. Vascular prostheses for aortocoronary bypass grafting: A review. Artif Organs 1995;19:39–45.
2. Ferrari ER, Von Segesser LK. Arterial grafting for myocardial revascularization: How better is it? Curr Opin Cardiol 2006; 21:584–588.
3. Zilla P, Bezuidenhout D, Human P. Prosthetic vascular grafts: Wrong models, wrong questions and no healing. Biomaterials 2007;28:5007–5027.
4. Pasquinelli G, Freyrie A, Preda P, Curti T, D'addato M, Laschi R. Healing of posthetic arterial grafts. Scanning Microsc 1990;4:351–362.
5. Isenberg BC, Williams C, Tranquillo RT. Small-diameter artificial arteries engineered in vitro. Circ Res 2006;98:25–35.
6. Doi K, Nakayama Y, Oka T, Matsuda T. A new microporous polyurethane vascular graft prepared by an excimer laser ablation technique. ASAIO J 1995;41:M608–M611.
7. Campbell JH, Efendy JE, Campbell GR. Novel vascular graft grown within recipient's own peritoneal cavity. Circ Res 1999; 85:1173–1178.
8. Pektok E, Nottelet B, Tille JC, Gurny R, Kalangos A, Moeller M, Walpoth BH. Degradation and healing characteristics of small-diameter poly (epsilon-caprolactone) vascular grafts in the rat systemic arterial circulation. Circulation 2008;118:2563–2570.
9. Nakayama Y, Ishibashi-Ueda H, Takamizawa K. In vivo tissue-engineered small-caliber arterial graft prosthesis consisting of autologous tissue (Biotube). Cell Transplant 2004;13: 439–449.

10. Sakai O, Kanda K, Ishibashi-Ueda H, Takamizawa K, Ametani A, Yaku H, Nakayama Y. Development of the wing-attached rod for acceleration of "Biotube" vascular grafts fabrication in vivo. J Biomed Mater Res B Appl Biomater 2007; 83:240–247.
11. Watanabe T, Kanda K, Ishibashi-Ueda H, Yaku H, Nakayama Y. Development of biotube vascular grafts incorporating cuffs for easy implantation. J Artif Organs 2007;10:10–15.
12. Kempen DH, Yaszemski MJ, Heijink A, Hefferan TE, Creemers LB, Britson J, Maran A, Classic KL, Dhert WJ, Lu L. Non-invasive monitoring of BMP-2 retention and bone formation in composites for bone tissue engineering using SPECT/CT and scintillation probes. J Control Release 2009; 134:169–176.
13. Hobo K, Shimizu T, Sekine H, Shin'oka T, Okano T, Kurosawa H. Therapeutic angiogenesis using tissue engineered human smooth muscle cell sheets. Arterioscler Thromb Vasc Biol 2008;28:637–643.
14. Mccarthy I. The physiology of bone blood flow: A review. J Bone Joint Surg Am 2006;88:4–9.
15. Brockmann MA, Kemmling A, Groden C. Current issues and perspectives in small rodent magnetic resonance imaging using clinical MRI scanners. Methods 2007;43:79–87.
16. Yamamoto A, Sato H, Enmi J, Ishida K, Ose T, Kimura A, Fujiwara H, Watabe H, Hayashi T, Iida H. Use of a clinical MRI scanner for preclinical research on rats. Radiol Phys Technol 2009;2:13–21.
17. Smith DA, Clarke LP, Fiedler JA, Murtagh FR, Bonaroti EA, Sengstock GJ, Arendash GW. Use of a clinical MR scanner for imaging the rat. Brain Res Bull 1993;31:115–120.
18. Guzman R, Lövblad KO, Meyer M, Spenger C, Schroth G, Widmer HR. Imaging the rat brain on a 1.5 T clinical MR-scanner. J Neurosci Methods 2000;97:77–85.
19. Huang H, Zhou YM, Ishibashi-Ueda H, Takamizawa K, Ando J, Kanda K, Yaku H, Nakayama Y. *In vitro maturation* of "Biotube" vascular grafts induced by a 2-day pulsatile flow loading. J Biomed Mater Res B Appl Biomater 2009 [Epub ahead of print].
20. Hayashida K, Kanda K, Yaku H, Ando J, Nakayama Y. Development of an in vivo tissue-engineered, autologous heart valve (the biovalve): Preparation of a prototype model. J Thorac Cardiovasc Surg 2007;134:152–159.
21. Hayashida K, Kanda K, Oie T, Okamoto Y, Sakai O, Watanabe T, Ishibashi-Ueda H, Onoyama M, Tajikawa T, Ohba K, Yaku H, Nakayama Y. "In vivo tissue-engineered" valved conduit with designed molds and laser processed scaffold. J Cardiovasc Nurs 2008;23:61–64.
22. Nakayama Y, Zhou YM, Ishibashi-Ueda H. Development of in vivo tissue-engineered autologous tissue-covered stents (biocovered stents). J Artif Organs 2007;10:171–176.

Ann Nucl Med (2010) 24:1–11
DOI 10.1007/s12149-009-0323-8

ORIGINAL ARTICLE

Development of motion correction technique for cardiac ^{15}O-water PET study using an optical motion tracking system

Kazuhiro Koshino · Hiroshi Watabe · Shinji Hasegawa · Takuya Hayashi · Jun Hatazawa · Hidehiro Iida

Received: 19 August 2009 / Accepted: 9 October 2009 / Published online: 3 December 2009

Abstract
Objective Cardiac ^{15}O-water PET studies provide an accurate quantitation of regional myocardial blood flow (rMBF). We developed a motion correction system using an optical motion-tracking device to detect a subject's global movement for cardiac study.
Methods PET studies were carried out on a cardiac phantom and a healthy volunteer at rest. The three-dimensional locations of the markers attached to the subjects during scans were measured using an optical motion-tracking system. In the phantom study, we performed a transmission scan and seven ^{18}F emission scans of a baseline and with artificial misalignment of shifts and rotations. The correlation coefficients between the baseline and the other images before and after the corrections for the misalignment were calculated. In the human study, we performed a ^{15}O-water dynamic scan with a transmission and axially 30 mm-shifted transmission scans. Motion of the subject was estimated by the information from the system, and was corrected on each sinogram using attenuation maps realigned to dynamic frames. Reconstructed dynamic images were then realigned to the transmission data. We calculated rMBF values for nine segments and myocardial images from the emission images, which were reconstructed with the first attenuation map (reference) and with the misaligned attenuation map before and after our corrections.
Results In the phantom study, the correlation coefficients were improved from 0.929 ± 0.022 to 0.987 ± 0.010 (mean $\pm$ SD) after the corrections. In the human study, the global and cyclic movements were detected. The cyclic movement due to respiration was smoothed by frame-averaging, and reasonable information of the global movement was obtained. The rMBF value (mean $\pm$ SD) was 0.94 ± 0.12 mL/min/g for the reference. The rMBF values using the misaligned attenuation map changed from 1.03 ± 0.21 to 0.93 ± 0.11 mL/min/g after the correction, and spurious defects in myocardial images were also recovered.
Conclusions Our technique provided reasonable information for correcting the global movement of the subject. It was shown that this system was applicable to detect and correct subject movement in cardiac PET studies at rest.

Keywords Myocardial blood flow · PET · Motion correction · Attenuation correction · ^{15}O-labeled water

K. Koshino (✉) · H. Watabe · H. Iida
Department of Investigative Radiology,
National Cardiovascular Center Research Institute,
5-7-1 Fujishirodai, Suita, Osaka 565-8565, Japan
e-mail: koshino@ri.ncvc.go.jp

S. Hasegawa
Department of Cardiology, Osaka Koseinenkin Hospital,
Osaka, Japan

T. Hayashi
Functional Probe Research Laboratory,
RIKEN Center for Molecular Imaging Science, Hyogo, Japan

J. Hatazawa
Department of Nuclear Medicine and Tracer Kinetics,
Osaka University Graduate School of Medicine, Osaka, Japan

Introduction

Motion of a patient during a positron emission tomography (PET) scan can cause deterioration in image quality and quantitative accuracy. Several techniques have been